CHALMERS

Investigation and design of high gain, low sidelobes, compact antennas at E - band

Master's Thesis in Antennas

Ioannis Papageorgiou

Department of Signals & Systems
Chalmers University of Technology
Gothenburg, Sweden 2012
Master's Thesis 2012:1

Abstract

This master thesis is about the investigation, design and evaluation of high gain, low sidelobe antennas in the E - band (71 - 86 GHz), which are intended for a multiple gigabit wireless system. The requirements of this E - band antenna is to have a gain higher than or equal to 38 dBi, a linear polarization and a Class 3 Radiation Pattern Envelope (RPE) according to ETSI. The return loss should be greater than 10 dB and the connector interface should be a rectangular waveguide. Several different antenna types are investigated and the two most attractive candidates are selected for further analysis, design and evaluation. These are a circular parabolic reflector antenna illuminated by a hat feed and an one dimensional parabolic reflector in a parallel plate structure, which illuminates the hat feed of a cylindrical reflector antenna.

Acknowledgements

I would like to thank my supervisors from the research department of Ericsson AB, Anders Derneryd and Lars Manholm for their constant help and support throughout the master thesis. Their ideas and guidance contributed a lot to the fulfillment of this project.

Moreover, I would like to thank my supervisor and examiner from Chalmers, associate professor Jian Yang, for his support and his creative ideas. His contribution to this project was equally important and he provided a lot help during the period of this master thesis.

Finally, I would like to thank the complete research department of Ericsson AB for giving me the opportunity to work on this master thesis and enhance my knowledge on the field of antennas in parallel with learning how to work and collaborate in an industrial environment.

Ioannis Papageorgiou, Sweden 23/6/12

Contents

1

Introduction

The increasing demand of line of sight (LOS) links with high data rates and long range, are enabled by the allocation of new frequency spectrum. In 2003 the Federal Communication Commision (FCC) allocated in US the E - band at $71 - 76$ GHz and $81 - 86$ GHz for radio link applications. This new frequency spectrum has a great potential for point to point wireless links and wireless backhaul applications [1].

The commercial E - band links are currently limited to data rates up to 1.25 Gb/s, however the 5 GHz bandwidth would allow data rates of up to 10 Gb/s with the use of higher modulation formats. The current E - band applications do not use high order modulation techniques but rather simpler ones, such as binary phase shift keying (BPSK), quadrature phase shift keying (QPSK) and amplitude shift keying (ASK). Moreover, E - band wireless links can replace fiber optics, because they are less costly and easier to deploy [2].

The antennas that are frequently used in E - band are required to be small, high gain, suitable for integration with the rest of the components. They should fulfill the ETSI requirements for minimum antenna gain of 38 dBi and radiation pattern envelope releases 2, 3 or 4 depending on applications. [3]. Several antennas in literature are studied and their performance results are compared in Chapter 2. Then, based on this study two potential candidates are further examined and a preliminary design is done in Chapter 3. Moreover, the simulation results of a detailed design are presented and discussed in Chapter 4 and finally, a limited tolerance study is presented in Chapter 5.

2

Survey of potential antenna candidates

For the requirements of this project that are shown in table 2.1, different types of antennas are examined and their characteristics are analyzed, in order to conclude the best candidate for further analysis and design. The antenna types that are taken into consideration are reflector antennas, microstrip antennas, lens antennas, horn antennas and horn arrays, as well as waveguide slot array antennas. Each one of them will be analyzed separately in the sub sections below.

Parameter	**Requirement**
Frequency	71 - 76 GHz and 81 - 86 GHz
Gain	$\geq$ 38 dBi
Polarization	Linear
Radiation pattern envelopes (RPE)	ETSI class 3
Return loss	$>$ 10 dB
Connector Interface	Rectangular waveguide

Table 2.1: Antenna requirements

2.1 Reflector antennas

Reflector antennas are very attractive candidates for use at high frequencies, because they have high gain and low losses. However, the size of a high gain reflector antenna can sometimes be too big to be practical in short range communication applications such as backhaul. There are quite a few companies worldwide that manufacture reflector antennas in the E - band. Most of their products are front-fed parabolic reflectors or cassegrain antennas and their dimensions depend on the gain.

Therefore, in order to achieve gain $G = 38$ dBi, the diameter d of a circular aperture can be calculated by (2.1)

$$G = e_A(\frac{\pi d}{\lambda})^2 \Leftrightarrow d = \sqrt{\frac{\lambda^2 G}{\pi^2 e_A}} \tag{2.1}$$

Typical values for the antenna efficiency e_A are between $0.5 - 0.7$. The diameter of the antenna varies in the range: 12.5 cm $-$ 15.1 cm within the frequency band for an antenna efficiency of 0.5. Usually when an antenna is designed in a wide frequency band, the diameter of the reflector is determined by the longest wavelength which corresponds to the lowest frequency. The gain of a circular aperture as a function of the diameter for an antenna efficiency of 0.5 is plotted in figure 2.1.

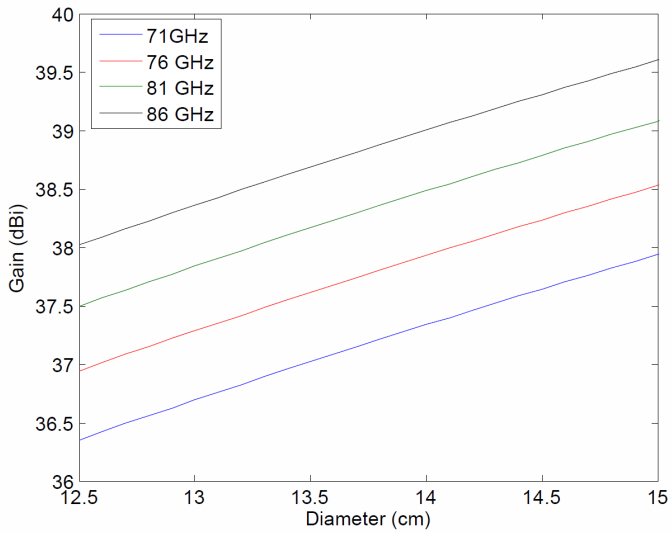

Figure 2.1: Gain towards antenna diameter for different wavelengths, assuming an antenna efficiency of 0.5

A 70 GHz Cassegrain antenna has been designed in [4] and the subreflector geometry is obtained by the Fourier - Jacoby surface expansion. For an antenna efficiency greater than 0.55 the gain of the antenna is between $43.3 - 43.5$ dBi. This corresponds to a

directivity of $D = 46$ dBi, as it can be calculated by equation (2.2)

$$G = e_A D \tag{2.2}$$

The dimensions of the double reflector antenna are 30 cm for the main reflector and 4 cm for the subreflector of the cassegrain antenna.

Another example of a cassegrain antenna in the same frequency band has been designed in [5]. This uses a 30 cm circular fresnel flat reflector as the main reflector and a subreflector with a hyperbolic shape, which is in that case as well determined by the Fourier - Jacoby expansion. The measured antenna gain is around 41.5 dBi.

Figure 2.2: Fresnel flat reflector [5]

In the frequency range of 76 - 77 GHz an anti collision radar system is implemented and it can be used in future car generations [6]. This system uses high gain reflector antennas of at least 30 dBi, in order to limit the transmitted power. Three different types of reflector antennas were simulated and their results were compared. One parabolic profile reflector and one reflector with synthesized profile; both with circular apertures and one reflector with an elliptic aperture and a synthesized profile.

The gain of the reflector antennas was around 40 dBi at $\theta = 5\,^\circ$ and more than 30 dBi at $\theta = 25\,^\circ$ and the diameter of the reflector antennas was around 16cm. The elliptic aperture reflector has the lowest side lobe level and the highest gain, thus the best performance in comparison with the others. The feeding source of the reflectors is an ideal conical horn antenna [6].

Finally, another design would be a cylindrical linear fed parabolic reflector whose feed is illuminated by a parallel plate structure. Inside the parallel plate could be an enclosed parabolic reflector, similar to [7] and this could be illuminated by a horn antenna or another type of feed, such as a hat feed. The parallel plate structure makes the antenna compact and the cylindrical shape of the reflector makes it easier to be manufactured than the one with the paraboloid shape.

A cylindrical parabolic reflector fed by a printed antenna array is designed at [8] in the frequency range of 57 - 64 GHz.The measured gain at 60 GHz is 34 dBi and the length of the cylindrical parabolic reflector is 100 mm. A photo of the realized antenna is shown in figure 2.3.

Figure 2.3: Cylindrical parabolic reflector, fed by printed antenna array [8]

In conclusion to the referred antenna designs, reflector antennas are strongly recommended to be used at high frequencies, due to their excellent performance characteristics in gain and efficiency.

2.2 Microstrip antennas

Microstrip antennas are widely used in telecommunications, because they are cheap to fabricate, they have a thin profile and light weight. Also, microstrip antennas have dual polarization capability and it is very easy to integrate them with other RF components. However, at high frequencies the losses of the substrate material increase and the gain of the microstrip antennas is limited. Low efficiency and narrow bandwidth (1 - 5%) are some more disadvantages of the microstrip antennas.

In general, the losses of microstrip antennas are hard to estimate precisely at very high frequencies. The directivity of the antenna, if the area of the aperture is known can be calculated by equation (2.3), assuming 100% illumination efficiency. Thus, the gain of a square antenna is defined as the directivity minus the feed line losses as it is shown in equation (2.4), assuming a parallel feed network.

$$D(dBi) = 10log(\frac{4\pi}{\lambda^2}A) \tag{2.3}$$

$$G(dBi) = D(dBi) - \alpha L = 10log(\frac{4\pi}{\lambda^2}A) - \alpha L = 10log(\frac{4\pi}{\lambda^2}L^2) - \alpha L \tag{2.4}$$

where, A is the square aperture area of the microstrip antenna and we assume that the aperture area is $A = L^2$.

Comparing equation (2.4) with equation (2.2) the losses can be related with the antenna efficiency such as:

$$e_A(dB) = -\alpha L \tag{2.5}$$

Therefore, for losses $\alpha = 15 - 60$ dB/m, the gain G of the antenna and the antenna efficiency e_A can be plotted as a function of the size L of the microstrip antenna, as it is shown in figure 2.4.

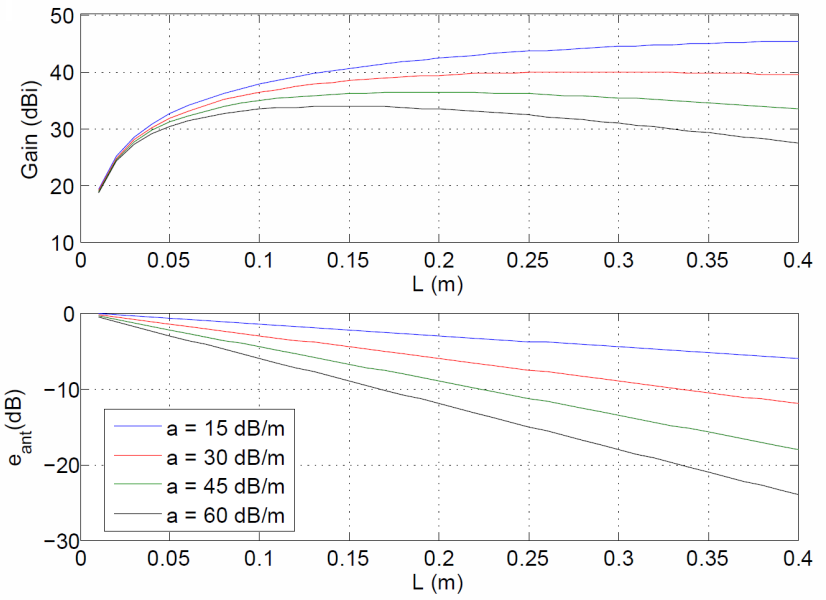

Figure 2.4: Gain and antenna efficiency towards the size (LxL) for different values of losses for the center frequency 78.5 GHz

It is noticed that for losses higher than about 25 dB/m the gain will always be under 38 dBi, no matter how big the aperture of the microstrip antenna is.

Several microstrip antennas have already been designed in the E - band from different substrate materials and they have different performance characteristics. However, none of the ones that will be presented can provide such high gain as 38 dBi.

Low Temperature Co-fired Ceramic (LTCC) is a very compact substrate technology, which enables multilayer fabrication, sometimes more than 70 layers. Microstrip antennas that are developed by LTCC technology are easily integrated with other RFIC technologies and they have excellent hermiticity. Moreover, antennas have low dielectric losses and low conductor losses, too [9][10].

A 77 GHz microstrip antenna based on LTCC technology is deisgned in [9] with a bandwidth of 6.75 GHz. The maximum gain of a single patch antenna element with dimensions 1.5mm x 1.5mm is around 6.2 dBi. However, an array of antenna antennas

can provide higher gain, although the design is going to be more complicated. A 2x2 array provides a gain, higher than 11 dBi and the directivity is 12.3 dBi in the frequency range $73 - 79$ GHz. Thus, from equation (2.2) the efficiency of the antenna array can be calculated and it is around 74%.

Maximum directivity of 29.3 dBi can be achieved by a 16x16 antenna array. This antenna has a gain higher than 28 dBi. The dimensions of the 16x16 antenna array can be calculated to be around 32mm x 32mm. Therefore, an array of more elements could provide much higher gain, but the complexity of the design would be higher.

Using the results of the figure 2.4, it occurs that for $G = 38$ dBi the dimensions of the microstrip array would be around 107mm x 107mm and the amount of elements would be 52x52. This means that the feeding network of the antenna should be extremely small, because there are too many elements in a small area, therefore it could be very complicated to fabricate such an antenna.

A microstrip antenna is designed on RO3003 substrate for the frequency band of $79 - 80$ GHz and the gain is around 27 dBi [11]. The radiation efficiency of this planar array is 0.78 and the array is fed by a parallel-series feeding network. The layout of this 16x32 array can be seen in figure 2.5. The choice of a parallel feeding network increases the losses and the series feeding reduces the bandwidth. The 16x1 sub-array has a length of 32.6 mm and the total aperture area is assumed to be around 32.6 mm x 66.3 mm. Thus, if the antenna was not fed in series, the feeding network would be so large that it would be difficult to design in the limited area between the radiating elements.

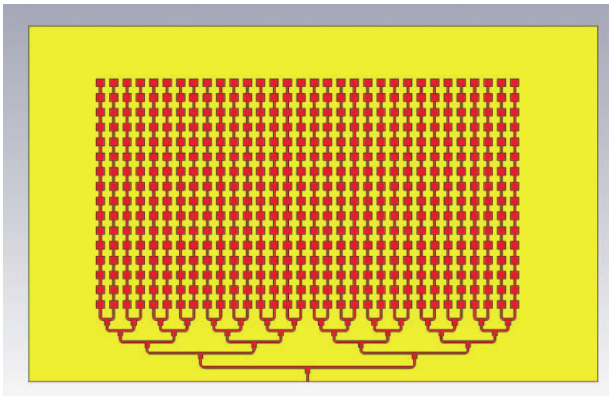

Figure 2.5: Layout of 16x32 microstrip array [11]

In order to achieve a gain of 38 dBi the array should include more elements and has a larger aperture area. By using figure 2.4 the area A would be around 10^{-6} m^2, therefore the dimensions of the layout would be 3.26 cm x 30.67 cm. It can be concluded that the array would be quite wide and unpractical and the losses would increase due to the parallel feeding network.

Furthermore, some aperture coupled microstrip antennas were designed in the frequency of 77 GHz on GaAs, using SiNx-membranes. The disadvantage of using semi-

conductor materials in antenna design is the reduced radiation efficiency, due to high permittivity [12][13]. An example of such an antenna is shown in figure 2.6. The choice of substrate materials in this multilayer fabrication process is independent and the optimization of the feed network can be done separately from the radiating element [13]. These are the only advantages towards conventional microstrip antennas.

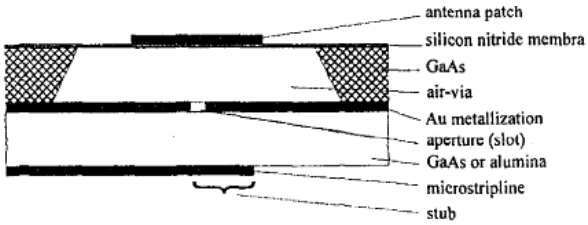

Figure 2.6: Microstrip antenna element on SiNx substrate [12]

A microstip antenna, usign a waveguide distributor in the frequency of 76.5 GHz is designed in [14]. The gain of the antenna is 28.7 dBi and since the calculated directivity is 35 dBi the total losses are $\alpha = 6.3$ dB. The bandwidth of the antenna is quite narrow, $76.3 - 76.7$ GHz and a configuration of the antenna can be shown in figure 2.7.

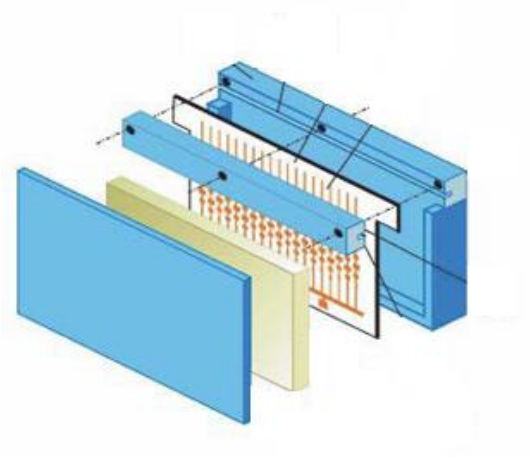

Figure 2.7: Microstrip antenna with waveguide distributor [14]

A planar quasi - Yagi antenna with folded dipole driver has also been designed in the frequency range $60 - 76$ GHz [15]. The design is compact and it is fabricated on low cost, low dielectric materials. The substrate that is used is Low Crystal Polymer (LCP) and the folded driver of the quasi - Yagi antenna reduces the spacing between the elements in array applications. For a single element, the gain is around $3 - 5$ dBi, which is quite low and the dimensions are 4mm x 5.8mm.

A linear array of four elements provides a gain of $8 - 9$ dBi and the dimensions of the array in that case, including the microstrip feed network are around 24mm x 10mm.

In the case of the demanding gain of 38 dBi the dimensions of the linear array would be around 900 mm x 10 mm, which is practically impossible. If the array was planar the dimensions would be 95 mm x 95 mm. Also, the losses in that case are even higher. Another drawback of the quasi - Yagi antenna is that the bandwidth of one element is quite narrow (around $3 - 4\%$) and it is not enough for many applications [15]. A schematic of the previously described quasi - Yagi antenna is shown in figure 2.8.

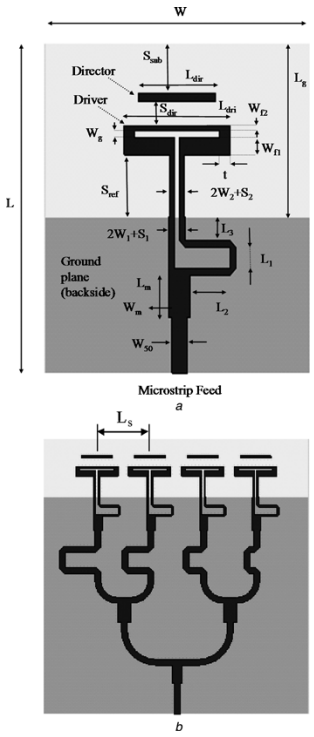

Figure 2.8: Quasi - Yagi antenna with folded dipole driver [15]

Moreover, a three beam antenna at 77 GHz for automotive applications is presented in [16]. The antenna is consisted of two parts, the feed network which has three waveguides and the microstrip antenna which is fabricated on Taconics TLY-5 material. The size of the 28x36 microstrip antenna is around 11.2cm x 9.1 cm. It provides a gain of 31 dBi and has a bandwidth of 1 GHz.

The frequency for automotive radar applications is $f = 77$ GHz and a patch antenna fed by coplanar waveguide (CPW) is designed in this frequency [17]. The fabrication of the antenna is done with the use of micromachining technology. The bandwidth is 9 GHz, which is quite wide (73.3 GHz - 82.3 GHz) and for a 2x1 patch array the bandwidth is 10 GHz. The size of each radiating patch is 1.7 mm x 1.7 mm. The substrate that is used is Corning Pyrex 7740. The advantages of this design are the low fabrication cost and the fact that there is freedom in selection of the substrate that is going to be used under the CPW. The gain of the single patch antenna is less than 10 dBi in the center

frequency and the size of the aperture is 1.7mm x 1.7mm.

2.3 Lens antennas

The use of lens antennas in millimeter wave applications has become more popular, because the dimensions of the lenses become smaller and they can be easily integrated with other components. Lens antennas have similar function as reflector antennas, because they have to be fed by a source which is usually a horn or a microstrip antenna or even an open waveguide [18].

In [19] a waveguide fed lens antenna is used to illuminate a reflector in the frequency range $30-90$ GHz. The diameter of the lens is around 75 mm and the directivity is 34.6 dBi. Also, the projected diameter of the reflector is 2.5 m and the directivity is 56.4 dBi. A schematic of the antenna can be seen in figure 2.9. Therefore, if the demanded gain is 38 dBi, the lens could be used alone with a diameter around 100 mm.

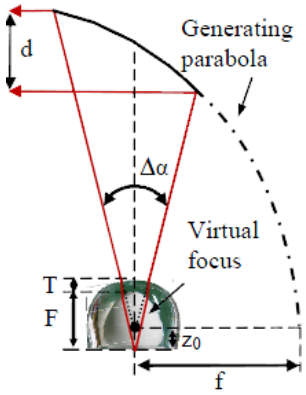

Figure 2.9: Lens fed by waveguide in combination with a reflector [19]

Moreover, an ultra-wide bandwidth (UWB) planar fed leaky lens antenna can be used in sub-millimeter wave frequencies [20]. The frequency range is $55-75$ GHz, the measured gain is around 20 dBi and the diameter of the lens is up to 100 mm.

An extended hempispherical lens coupled slot antenna is studied in [21]. A hemispherical lens is easier to fabricate than an elliptical lens and the slot antenna has a simple structure, therefore it can be easily fabricated as well. The gain of the antenna is $G = 31.5$ dBi for the frequency $f = 94$ GHz. The material of which the hemispherical lens coupled slot antenna is made of, is fused quartz.

The half - Maxwell fish-eye lens presented in [22] consists of three dielectric hempisherical cylinders. It provides a gain of 21.7 dBi in the frequency range of $76-81$ GHz. The lens is fed by a waveguide and the manufacturing of the materials is difficult, that is why lenses are not so attractive to be used in millimeter and sub - millimeter wave applications.

2.4 Horn antennas and horn arrays

Horn antennas are very simple and they are often used in many applications worldwide. They are also used as feed antennas for reflectors and lenses. There are several types of horn antennas and the equations for calculating the gain and the radius are slightly different. For a single pyramidal horn antenna the gain can be calculated by equation (2.6)

$$G = \frac{4\pi A}{\lambda^2} e_A \tag{2.6}$$

Therefore, in the E - band for gain $G = 38$ dBi and antenna efficiency $e_A = 0.5$ (the typical value for horns is around $0.4 - 0.8$) the area of the horn antenna will be around A = 1.79 cm^2 - 1.22 cm^2. If both sides of E and H aperture planes are equal the dimension of the aperture area would be 13.4 cm - 11 cm. Moreover, if the horn was conical, the gain would be calculated by equation(2.1), which is reproduced below.

$$G = (\frac{\pi d}{\lambda})^2 e_A \tag{2.7}$$

The diameter of the aperture area of the horn would be around d = 15.2 cm - 12.5 cm.

Another drawback of using a single horn antenna in such high frequencies is the fact that it will be very long. For a conical horn antenna, the optimal length L is calculated by equation (2.8)

$$d = \sqrt{3\lambda L} \Leftrightarrow L = \frac{d^2}{3\lambda} \tag{2.8}$$

For diameter values that were calculated by equation (2.7), the length of the horn will be $L = 1.78 - 1.49$ m. This long length shows that such a horn is impractical to use.

However, horn antennas can be used as elements in array antennas in order to achieve high gain and directivity. A planar antenna array radiating in E - band and consisting of horn elements is described in [23]. The array consists of 64x64 elements and the total dimensions are 25cm x 25cm x 9cm. The feeding network uses waveguide technology and it is shown in figure 2.10.

The antenna array provides a very high gain $G \geq 41$ dBi and its bandwidth is very broad, around 20%.

Moreover, a stacked patch fed horn antenna is presented in [24]. Multiple patches on top of each other are usually desinged in order to achieve higher bandwidth, therefore the antenna consists of a horn antenna, a CPW transition and two patch antennas. The gain of the antenna is around 12 dBi, the bandwidth is very broad, around 30% and the operation frequency is 94 GHz.

A pyramidal horn array of 32 elements is designed in [25] at the frequency of 76 GHz. The array is fed by a five stage power divider and it is used for collision avoidance systems in vehicles.

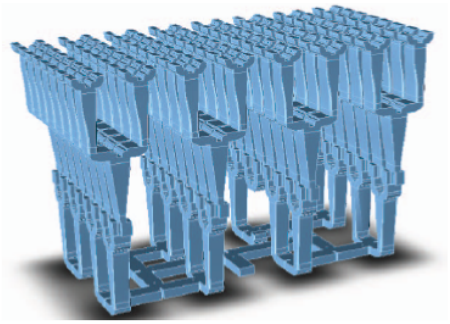

Figure 2.10: Subarray feeding network [23]

Furthermore, SSFIP(Strip-Slot-Foam-Inverted Patch) - horn antennas operating at 75 GHz are designed in [26] and [27]. The antennas are consisted of two parts, a silicon wafer and a Pyrex wafer as it can be seen in figure 2.11.

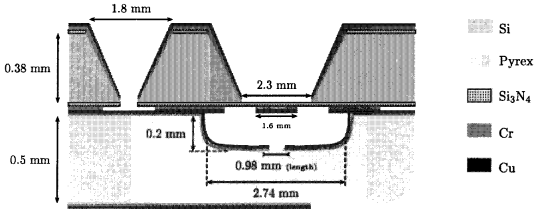

Figure 2.11: Integrated horn antenna at 75 GHz [26]

Each wafer is designed separetely and the silicon wafer is connected on top of the pyrex wafer by using micromachining technology.

Finally, a corrugated platelet horn is designed in [28]. The horn has an internal tilt in order to steer the beam several degrees. The fabrication of such an antenna is easy and has a low cost and it provides a gain of 20 dBi in the frequency range of $75 - 110$ GHz.

2.5 Slot array antennas

Waveguide slot arrays are very attractive candidates, because they have high directivity, low cross - polarization, low losses and high power handling capability. Many compact slot array antennas have been already designed in the E - band, mostly for automotive applications. Equation (2.3) that was used in microstrip arrays can approximately be applied in this case to relate the gain of the antenna with the dimensions of the aperture.

Post wall waveguide fed parallel plate slot arrays are discussed and designed in [29], [30] and [31]. These antennas are used for car - radar applications in the frequency range of $76 - 77$ GHz. They provide a gain of 29.6 dBi and they have an aperture efficiency

$e_A = 0.45$. The size of the aperture is 52mm x 49mm and a substrate of dielectric PTFE and glass fibers is used. A schematic of the slot array is shown in figure 2.12.

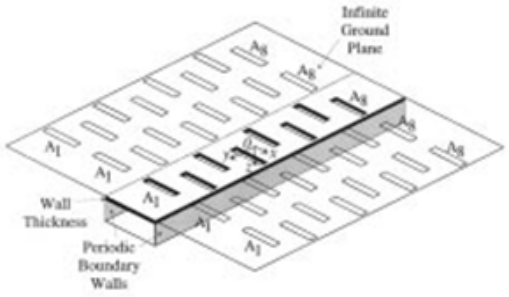

Figure 2.12: Parallel plate slot array [30]

The slot array that was designed has already sidelobe suppresion and high gain, however, in order to increase the gain, the aperture area needs to be increased as well. Thus, in order to achieve gain of 38 dBi , the size of the aperture area should be around 13cm x 13 cm, according to equation (2.3). This makes the antenna too big in size and more complicated to manufacture.

A similar design of a single - layer slotted waveguide array is shown in [32] at the band of 76 GHz. The gain is $G = 34.5$ dBi, the efficiency is $e_A = 0.5$ and the aperture area is around 81mm x 87mm. A schematic of the antenna is shown in figure 2.13.

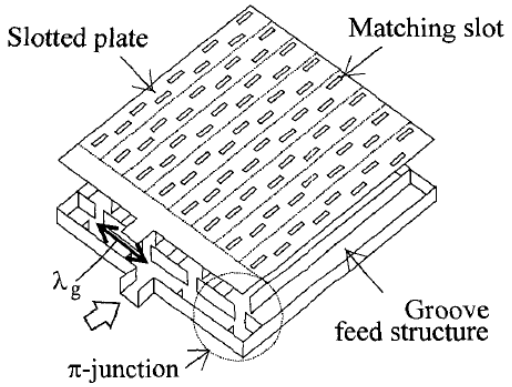

Figure 2.13: Single - layer slotted waveguide array[32]

Similarly to the case of the parallel plate slot array in order to achieve a gain as high as 38 dBi, the size of the aperture of the single - layer slotted waveguide array should be around 12.5cm x 12.5cm.

A single mode post-wall waveguide suitable for automotive radars is presented in [33]. The operating frequency of the antenna is 77 GHz and the measured gain is $24.4dBi$. The antenna efficiency is 0.67 for an aperture size of 55mm x 9.2mm and the antenna

is fabricated on a PTFE substrate. The transmission loss of the antenna is measured to be 0.2 dB/cm and it is much less than the transmission loss of the microstrip line. However, in order to achieve a gain of 38 dBi, the aperture size of the antenna should be larger.

A 16x16 quasi double-layer slot array antenna is presented in [34] in the center frequency of 83.5 GHz. The antenna is consisted of 16 4x4 subarrays which have wideband characteristics. The measured gain of the designed antenna is 32.4 dBi and the antenna efficiency is 0.83. The dimensions of the square aperture are 44.8mm x 48mm and the complete size of the antenna is 60mm x 60mm. The antenna is fabricated by diffusion bonding of copper plates and it can be seen in figure 2.14.

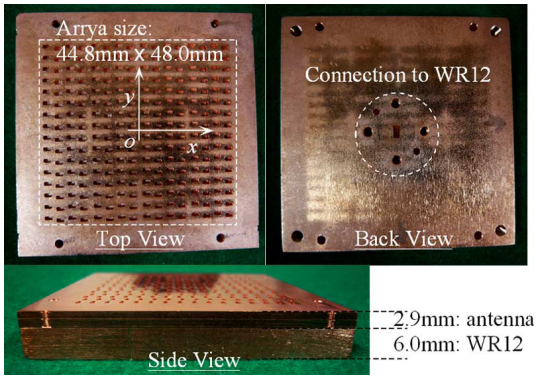

Figure 2.14: E-band uniform slot array fabricated on thin copper plates [34]

As in the previous cases that were presented in order to have a gain of 38 dBi, the aperture area of the antenna should be around 8.8cm x 8.8cm.

Another antenna for automotive radar applications is presented in [35] at 77 GHz. The antenna is made of two Rogers 5880 substrates and the lower substrate consists of a horn which is illuminating a parallel plate integrated parabolic reflector as shown in figure 2.15. The antenna provides a gain of 24 dBi for an efficiency of 0.5 and the overall size is around 50mm x 50mm.

For a gain of $38dBi$ the aperture size would be approximately equal with 12.3 cm x 12.3cm.

The technology of substrate integrated waveguide (SIW) is proposed and a 79 GHz slot antenna based on SIW is presented in [36]. Three different types of slot antennas were developed, a single slot, a longitudional slot array and 4x4 slot array antenna. The gain varies from 2.8 dBi - 11 dBi, with the latest antenna configuration to provide the maximum gain. Finally, the bandwidth varies from $4.7\% - 10.7\%$.

A 16x16 ceramic planar array antenna at 77 GHz is designed in [37]. This antenna uses laminated waveguides for feeding lines and has a wide bandwidth. The aperture size is 58.5mm x 58.5mm and the feed network consists of 3 layers. The material that it is used is low temperature co-firing ceramics and the antenna provides a gain of around 29.5 dBi for an efficiency of 0.33.

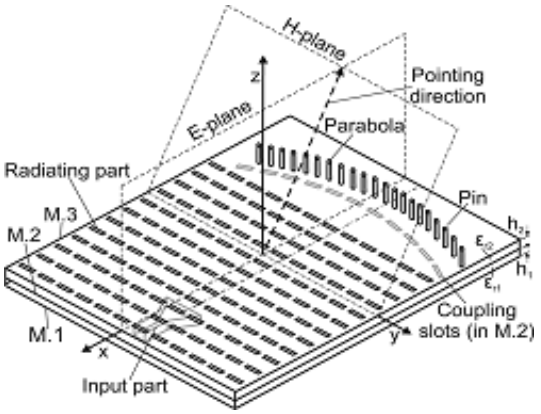

Figure 2.15: Top view of single-folded leaky wave antenna [35]

Finally, an alternating phase fed slotted waveguide with wide chokes at 76 GHz is presented in [38]. The maximum gain of the antenna is 34.4 dBi for an efficiency of 0.5. The size of the aperture area is 81mm x 84mm and for a gain of 38 dBi the size of the aperture should be around 12.5cm x 12.5cm. A schematic of the antenna structure is shown in figure 2.16.

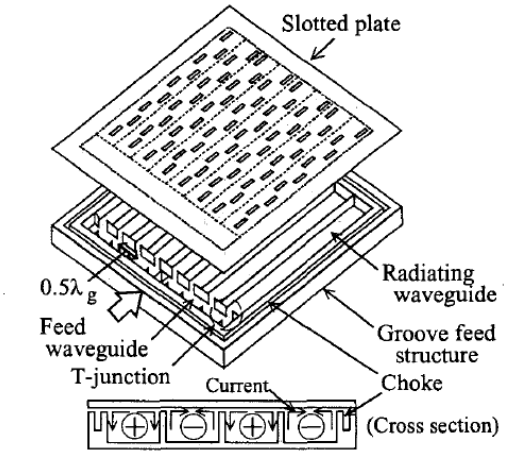

Figure 2.16: Alternating phase fed slotted waveguide antenna with wide chokes [38]

2.6 Possible antenna candidates

A summary of the most promising antenna candidates, from the ones that were presented in the previous sections, which are compact and provide high gain is shown in table 2.2.

Technology	Size	Gain	Efficiency	Frequency
Reflector [6]	$\phi = 160$ mm	40 dBi	0.5	76 - 77 GHz
Microstrip [9]	25.5mm x 25.5mm	28 dBi	0.74	73 - 79 GHz
Lens [20]	$\phi = 100$ mm	20 dBi	0.5	55 - 75 GHz
Horn array [23]	250mm x 250mm x 90mm	43 dBi	0.4	71 - 86 GHz
Waveguide [32]	81mm x 87mm	34.5 dBi	0.5	76

Table 2.2: Selected antenna candidates

Some of the antennas from table 2.2 do not give a gain of 38 dBi. Therefore, these antennas with their aperture dimensions modified in order to achieve a gain of 38 dBi are presented in table 2.3, in order to have a direct comparison that would help the selection of the best candidates. It is concluded that the reflector antennas are the most attractive candidates to be designed for high gain in the E - band.

Technology	Size	Efficiency	Frequency
Reflector	$\phi = 160$ mm	0.5	76 - 77 GHz
Microstrip	107mm x 107mm	0.74	73 - 79 GHz
Lens	$\phi = 760$ mm	0.5	55 - 75 GHz
Horn array	250mm x 250mm x 90mm	0.4	71 - 86 GHz
Waveguide	125 mm x 125 mm	0.5	76

Table 2.3: Selected antenna candidates with gain equal to 38 dBi

3

Preliminary design of selected antennas

In the previous section the most promising candidates were presented and two final antennas are selected to be designed from the ones of table 2.3. Both of the selected antennas are reflector antennas, due to their attractive characteristics in gain and aperture efficiency.

The first design is a front - fed circular parabolic reflector antenna with a hat feed and the second design is a cylindrical reflector illuminated by a linear hat feed which is fed by a parallel plate structure that includes an one dimensional reflector. Due to the requirements of this project the gain of the antenna should be ≥ 38 dBi. A fade margin of 2 dB can be assumed, thus the antennas can be preliminary designed for a gain of 40 dBi.

3.1 Circular reflector antenna with hat feed

The diameter of the circular parabolic reflector is determined by the longest wavelength which corresponds to the frequency of 71 GHz. From equation (2.1), the diameter of the reflector is found to be $d = 19.02$ cm for an antenna efficiency of 0.5 and a gain of 40 dBi. Then, the ratio of the focal point over the reflector diameter F/d needs to be determined. The initial assumption was $F/d = 0.3$, so $F = 57.06$ mm, which gives a half subtended angle $\theta_0 = 79.61°$ from equation (3.1) [39].

$$d = 4F\tan(\theta_0/2) \Leftrightarrow \theta_0 = 2\arctan(\frac{d}{4F}) \tag{3.1}$$

However, after further analyses and simulations it occurred that the half subtended angle needed to be larger in the case of a hat feed design and reduce spillover losses. Therefore the design of the antenna was done for $\theta_0 = 105°$. From equation (3.1),

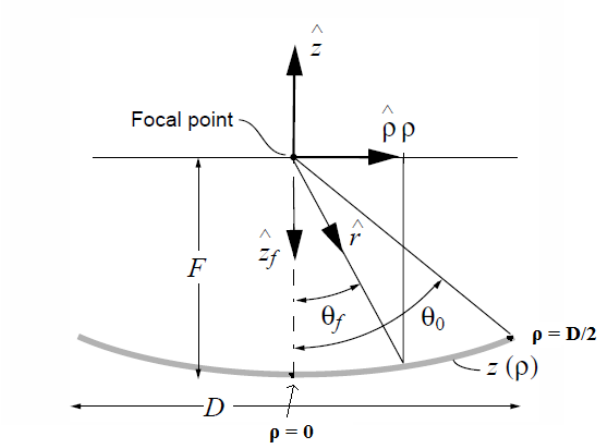

Figure 3.1: Geometry of rotational symmetric paraboloid [39]

$F = 36.5$ mm and $F/d = 0.19$. Moreover, the depth of focus Δz is calculated by (3.2) and (3.3).

$$z(\rho) = -F + \frac{\rho^2}{4F} \tag{3.2}$$

$$\Delta z = z_2 - z_1 = z(\rho_2) - z(\rho_1) = -F + \frac{\rho_2^2}{4F} - (-F + \frac{\rho_1^2}{4F}) = \frac{d^2}{16F} \tag{3.3}$$

for $\rho_1 = 0$ and $\rho_2 = d/2$ as it is shown in figure 3.1 and the depth of focus is $\Delta z = 61.9$ mm.

A complete schematic of the circular reflector antenna that was designed is shown in figure 3.2.

Furthermore, the feed illumination taper needs to be selected and this choice affects the final result of the aperture efficiency. If the aperture distribution is assumed to be truncated Gaussian, then figure 3.3 shows the relation between the relative radiation level and $(d/\lambda)sin(\theta)$ for different illumination taper values.

From figure 3.3 for d = 190 mm and $\lambda = 4.2$ mm (at 71 GHz), d/$\lambda = 45$ and then, the directivity towards angle θ is calculated and plotted in figure 3.4 , for different taper values. The ETSI class 3 sidelobe level is plotted as well in the same figure [3]. Therefore, for a selected taper of 10 dB, the sidelobe level of the truncated Gaussian is 8 - 10 dB below ETSI class 3, which is one of the requirements of this project. Finally, from the same figure, the half beamwidth is around 0.7°, so the θ_{3dB} beamwidth is expected to be twice that, i.e. 1.4°.

The theoretical aperture efficiency and the theoretical spillover efficiency can be determined by figures 3.5 and 3.6 [39]. For the selected subtended angle of 105°, the total aperture loss is around -1.7 dB and the spillover loss is around -0.3 dB. Finally,

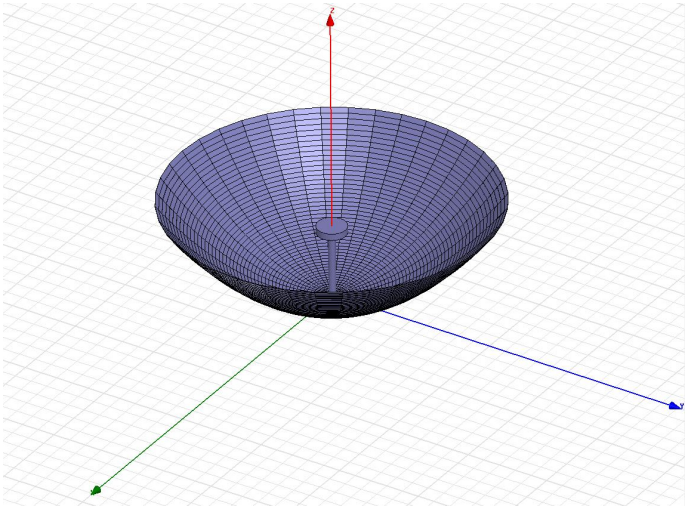

Figure 3.2: Circular parabolic reflector illuminated by a hat feed

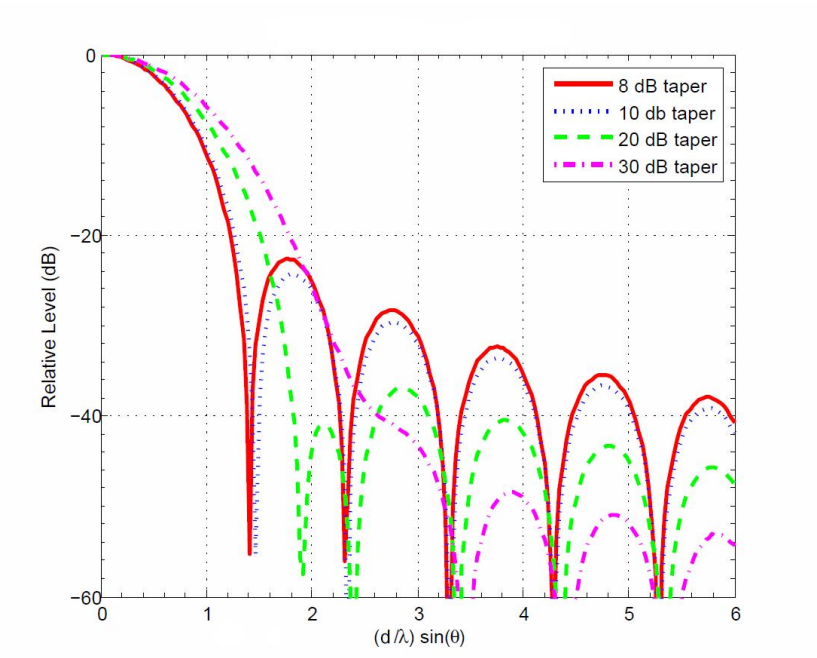

Figure 3.3: Universal radiation pattern of truncated Gaussian [39]

the blockage loss can be determined from figure 3.7, for the taper of 10 dB. If the ratio of the hat diameter over the reflector diameter is assumed to be 0.1, then the blockage loss is around -0.15 dB [39].

The calculation of the subefficiencies of a parabolic reflector antenna is done analyt-

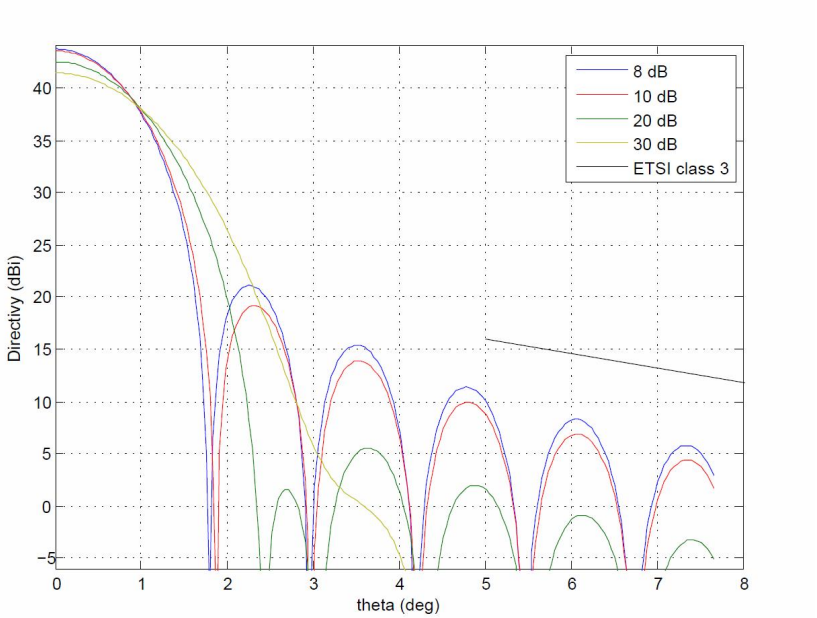

Figure 3.4: Directivity towards angle θ for a circular parabolic reflector

ically in [39] and the results are presented in equations (3.4) - (3.7) below. θ_0 is the half subtended angle and G_{co45}, as well as G_{xp45}, are the co and cross polarized feed pattern in the 45° plane, respectively.

The spillover efficiency is

$$e_{sp} = \frac{2\pi \int_0^{\theta_0}[|G_{co45}(\theta)|^2 + |G_{xp45}(\theta)|^2]sin\theta \, \mathrm{d}\theta}{2\pi \int_0^{\pi}[|G_{co45}(\theta)|^2 + |G_{xp45}(\theta)|^2]sin\theta \, \mathrm{d}\theta} \tag{3.4}$$

The polarization sidelobe efficiency is

$$e_{pol} = \frac{\int_0^{\theta_0}|G_{co45}(\theta)|^2 sin\theta \, \mathrm{d}\theta}{\int_0^{\theta_0}[|G_{co45}(\theta)|^2 + |G_{xp45}(\theta)|^2]sin\theta \, \mathrm{d}\theta} \tag{3.5}$$

The illumination efficiency is

$$e_{ill} = 2cot^2(\frac{\theta_0}{2})\frac{[\int_0^{\theta_0}|G_{co45}(\theta)|tan(\frac{\theta}{2}) \, \mathrm{d}\theta]^2}{\int_0^{\theta_0}|G_{co45}(\theta)|^2 sin\theta \, \mathrm{d}\theta} \tag{3.6}$$

And finally, the phase efficiency is

$$e_{\phi} = \frac{|\int_0^{\theta_0} G_{co45}(\theta)tan(\frac{\theta}{2}) \, \mathrm{d}\theta|^2}{[\int_0^{\theta_0}|G_{co45}(\theta)|tan(\frac{\theta}{2}) \, \mathrm{d}\theta]^2} \tag{3.7}$$

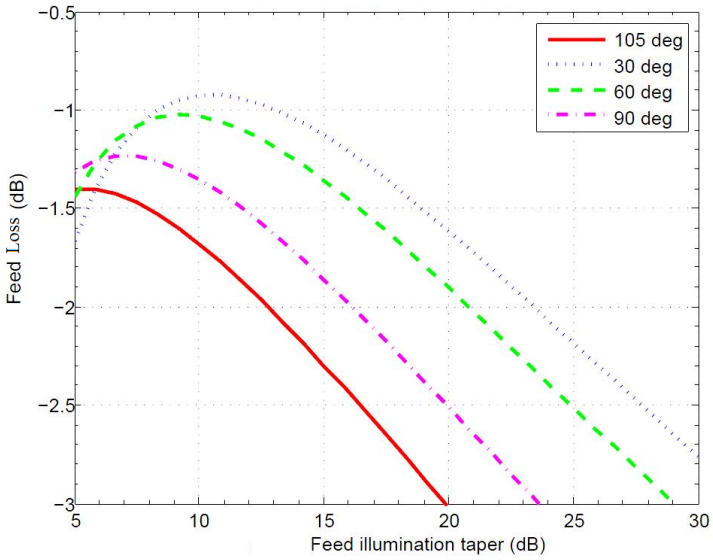

Figure 3.5: Feed illumination loss [39]

3.1.1 Theoretical directivity of circular reflector antenna

The theoretical directivity of a circular aperture is calculated by several equations from chapters 7 and 9 of [39], which are shortly presented below. Firstly, the aperture field can be constructed from the far-field function of E and H planes, $G_E(\theta)$ and $G_H(\theta)$, respectively. The aperture field is constructed in equation (3.8).

$$E_E(\rho) = -\frac{1}{F} cos^2(\theta/2) G_E(\theta) e^{-j2kF} \tag{3.8}$$
$$E_H(\rho) = -\frac{1}{F} cos^2(\theta/2) G_H(\theta) e^{-j2kF}$$

for $\rho < D/2$, where F is the focus of the reflector and θ the half subtended angle.

Then the co - polar and the cross polar of the 45° plane are constructed in equation (3.9).

$$E_{co45}(\rho) = \frac{1}{2}[E_E(\rho) + E_H(\rho)] \tag{3.9}$$
$$E_{co45}(\rho) = \frac{1}{2}[E_E(\rho) - E_H(\rho)]$$

The far-field function of the 45° plane of the circular aperture is proportional to equation (3.10).

$$G_{co45}(\theta) \sim \boldsymbol{E_{co45}}(\theta) cos^2(\theta/2) \tag{3.10}$$

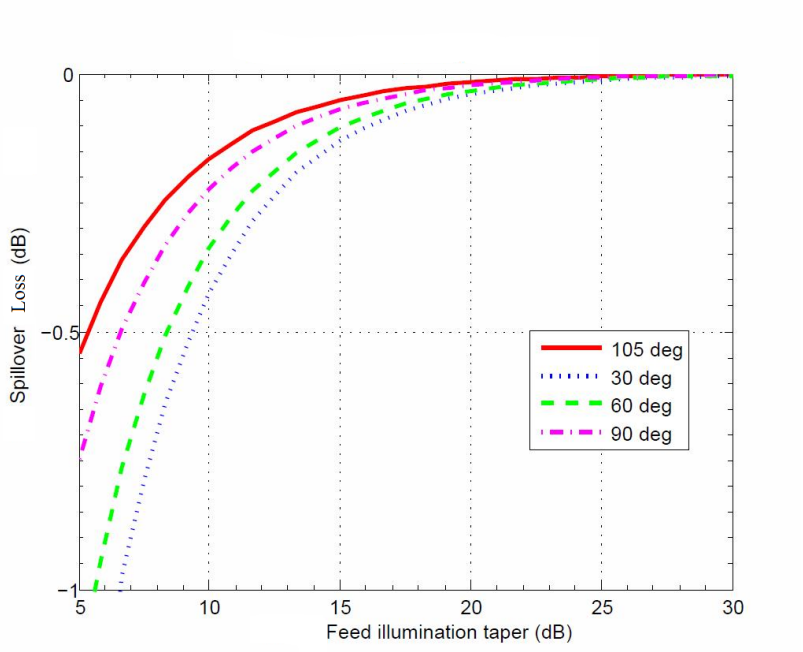

Figure 3.6: Spillover loss [39]

$$G_{xp45}(\theta) \sim \boldsymbol{E_{xp45}}(\theta) cos^2(\theta/2)$$

where

$$\boldsymbol{E_{co45}}(\theta) = 2\pi \int_0^{d/2} E_{co45}(\rho) J_0(k\rho sin\theta)\rho \, \mathrm{d}\rho \tag{3.11}$$

$$\boldsymbol{E_{xp45}}(\theta) = 2\pi \int_0^{d/2} E_{xp45}(\rho) J_2(k\rho sin\theta)\rho \, \mathrm{d}\rho$$

Therefore the total directivity of the circular aperture is calculated by equation (3.12)

$$D = \frac{4\pi |G_{co45}|^2_{max}}{P} \tag{3.12}$$

and P is the power calculated in equation (3.13)

$$P = 2\pi \int_0^{\pi} [|G_{co45}(\theta)|^2 + |G_{xp45}(\theta)|^2] sin\theta \, \mathrm{d}\theta \tag{3.13}$$

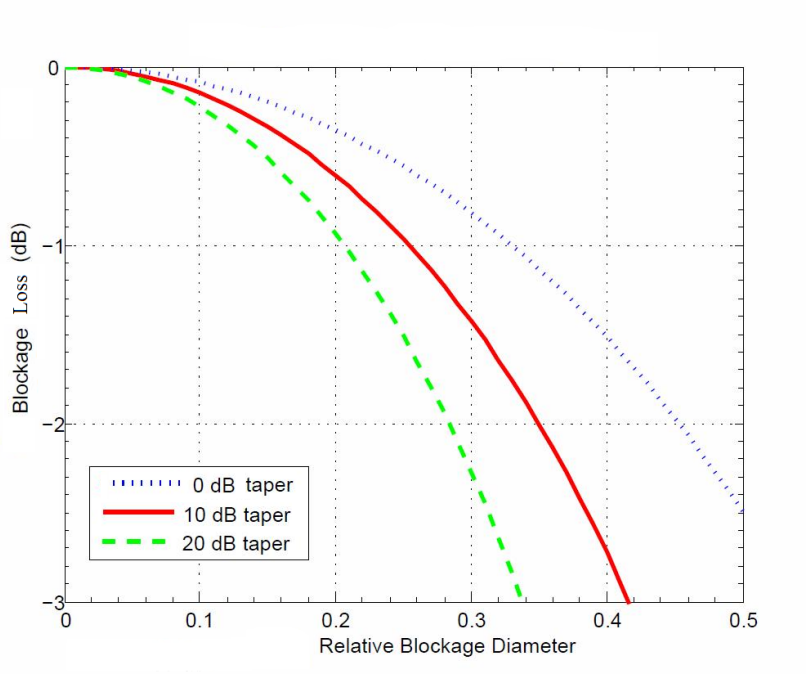

Figure 3.7: Blockage loss [39]

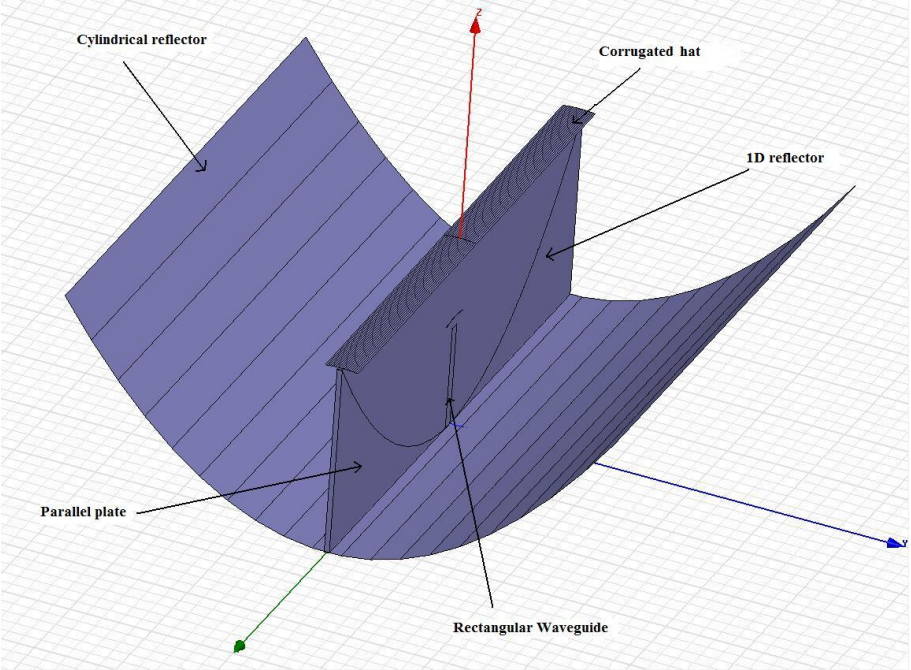

Figure 3.8: Cylindrical parabolic reflector

3.2 Cylindrical reflector antenna

The second antenna design is a cylindrical reflector that is fed by a corrugated hat line feed, which is fed by a parallel plate structure. Inside the parallel plate there is an one dimensional reflector antenna, which is also fed by a hat feed. The complete schematic of the antenna can be seen in figure 3.8.

In this case, the aperture area is rectangular in contrast with the circular reflector antenna. For simplicity, the aperture area is selected to be square and its dimensions can be found by equation 2.4. An antenna efficiency of 0.5 is selected and the assumed gain is 40 dBi. For the longest wavelength the area is $A = 2.84$ dm^2, thus each side is 168.37 mm long. The subtended angle for both reflectors is selected to be 105°, similar to the case of the circular reflector and F = 32.3 mm from equation (3.1). Therefore, $F/d = 0.19$ and the depth of focus is calculated to be $\Delta z = 54.85$ mm from equations (3.2) and (3.3).

In that case as well the feed illumination taper that is selected is 10 dB and the directivity towards angle θ, is plotted in figure 3.9, for d = 168.37 mm and $\lambda = 4.2$mm, so $d/\lambda = 40$. It is noticed that the sidelobe level is 10 dB lower than ETSI class 3 and the half beamwidth is $0.6° - 0.7°$, i.e. the θ_{3dB} beamwidth is $1.2° - 1.4°$. Both reflectors of the cylindrical reflector design are identical, apart from the shape of the hat that is feeding them.

The figures that relate the feed illumination taper with the aperture, spillover and

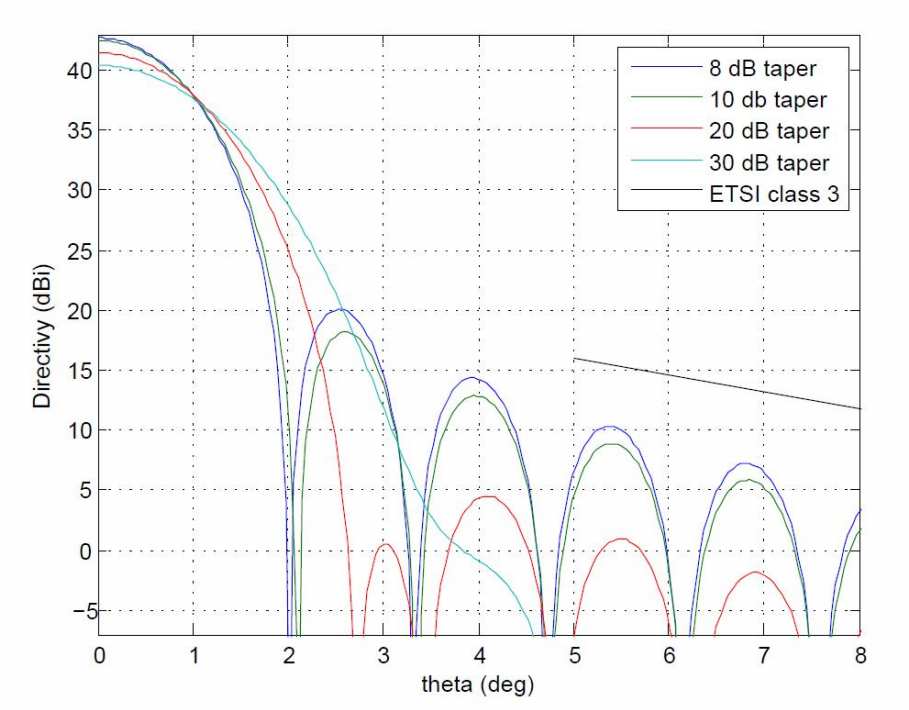

Figure 3.9: Directiviry towards angle θ for the rectangular aperture cylindrical reflector

blockage efficiency cannot be directly applied to this design, because they are only valid for rotationally symmetric reflectors.

3.2.1 Theoritical directivity and far-field function of cylindrical reflector

The far-field function of the rectangular aperture can be calculated analytically, assuming that the aperture distribution is truncated Gaussian. The general expression of the free space far - field function is shown in equation (3.14) and depends on the one dimensional Fourier transforms of the aperture distributions [39].

$$G(\theta,\phi) = -2C_k cos^2(\frac{\theta}{2})(cos\phi\boldsymbol{\theta} - sin\phi\boldsymbol{\phi})E_{ax}(ksin\theta cos\phi, ksin\theta sin\phi) \tag{3.14}$$

$$-2C_k cos^2(\frac{\theta}{2})(sin\phi\boldsymbol{\theta} - cos\phi\boldsymbol{\phi})E_{ay}(ksin\theta cos\phi, ksin\theta sin\phi)$$

and $C_k = \frac{-jk}{4\pi}$
For y - polarization the far- field function is proportional to

$$E_{ay}(ksin\theta cos\phi, ksin\theta sin\phi) = E_{ay}(k\boldsymbol{x}\boldsymbol{r}, k\boldsymbol{y}\boldsymbol{r}) = A(k\boldsymbol{x},\boldsymbol{r})B(k\boldsymbol{y},\boldsymbol{r})$$

with

$$A(k\boldsymbol{x},\boldsymbol{r}) = \int_{-d/2}^{d/2} e^{-(x/\rho_\alpha)^2} e^{(jkx\boldsymbol{xr})}\,\mathrm{d}x$$

and

$$B(k\boldsymbol{y},\boldsymbol{r}) = \int_{-d/2}^{d/2} e^{-(y/\rho_\alpha)^2} e^{(jky\boldsymbol{yr})}\,\mathrm{d}y$$

where ρ_a is the 1/e radius or $\rho_a = \frac{d}{2\sqrt{0.4\ln 10}}$, for 10 dB of illumination taper.

The directivity of the rectangular aperture of the cylinder can be calculated by equation (3.15), similar to (3.12) [39].

$$D = \frac{4\pi|G|^2_{max}}{P} \tag{3.15}$$

The maximum of the absolute of the far - field is proportional to the maximum of the one dimensional Fourier transforms and this occurs for $\theta = 0$. Thus,

$$A(k\boldsymbol{x},\boldsymbol{r}) = A(ksin\theta cos\phi, ksin\theta sin\phi) = e^{(1/2k\rho_\alpha sin\theta\cos\phi)^2} \int_{-d/2}^{d/2} e^{-(\frac{x}{\rho_\alpha})^2} e^{(jk\rho_\alpha(sin\theta cos\phi))^2}\,\mathrm{d}x$$

For $\theta = 0$,

$$A(0,0) = \int_{-d/2}^{d/2} e^{-(\frac{x}{\rho_\alpha})^2}\,\mathrm{d}x = \sqrt{\pi}\rho_\alpha erf(\frac{d}{2\rho_\alpha})$$

$B(k\boldsymbol{y},\boldsymbol{r})$ gives the same result, so the maximum value of the far - field function is proportional to the maximum value of the aperture integral function.

$$G_{max} \sim E_{ay}(k\boldsymbol{xr}, k\boldsymbol{yr})_{max} = \pi\rho_\alpha^2 erf^2(\frac{d}{2\rho_\alpha})$$

The total power of the far - field function is equal with the square of the aperture integral function.

$$P = \int_{-d/2}^{d/2}\int_{-d/2}^{d/2} |E_{ay}(k\boldsymbol{xr}, k\boldsymbol{yr})|^2\,\mathrm{d}x\mathrm{d}y = \int_{-d/2}^{d/2}\int_{-d/2}^{d/2} e^{-2(\frac{x}{\rho_\alpha})^2-2(\frac{y}{\rho_\alpha})^2}\,\mathrm{d}x\mathrm{d}y = \frac{\pi}{2}\rho_\alpha^2 erf^2(\frac{\sqrt{2}d}{2\rho_\alpha})$$

Therefore, the total directivity that is calculated by equation (3.15) is

$$D = \frac{4\pi}{\lambda^2}\frac{[\pi\rho_\alpha^2 erf^2(\frac{d}{2\rho_\alpha})]^2}{\frac{\pi}{2}\rho_\alpha^2 erf^2(\frac{\sqrt{2}d}{2\rho_\alpha})} = \frac{4\pi}{\lambda^2}\frac{erf^4(\frac{d}{2\rho_\alpha})}{erf^2(\frac{\sqrt{2}d}{2\rho_\alpha})} \tag{3.16}$$

The final conclusion is that the directivity depends only on the wavelength and the dimension d of the aperture area. For the different wavelengths in the E-band and an antenna diameter of 168.37 mm, the directivity of the aperture within blockage is calculated by equation (3.16) and it is plotted as a function of the frequency in figure 3.10.

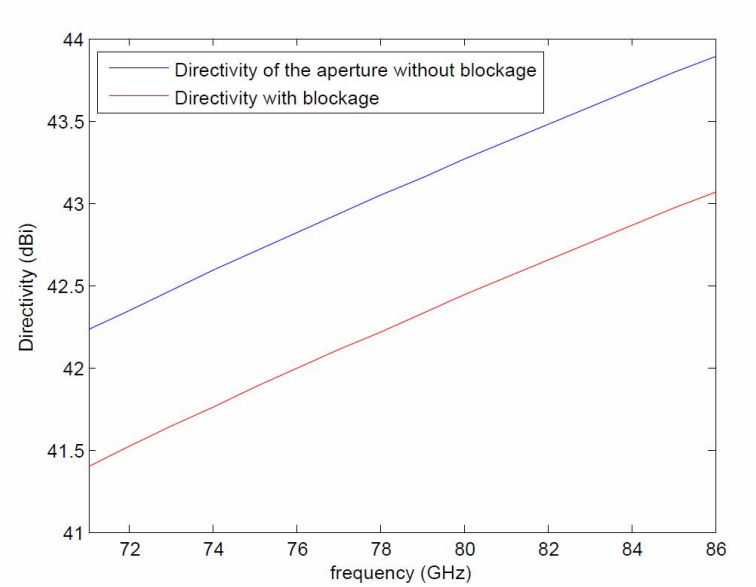

Figure 3.10: Directivity along frequency for a square aperture

3.2.2 Total blockage of the cylindrical reflector

The blockage of the hat feeds of the cylindrical reflector design is different from the usual blockage that typical hat feeds cause, such as in the case of the circular parabolic reflector. In this case the blockage of the rectangular aperture is along two dimensions. The blockage at the first dimension comes from the hat feed inside the parallel plate and the blockage at the second dimension comes from the line feed that is extended along the aperture of the parallel plate.

A schematic of the blockage in the rectangular aperture is shown in figure 3.11. The black area in the center is the hat feed of the parallel plate that is responsible for the blockage in one dimension and together with the gray area, they contribute to the total blockage of the rectangular area. It is also assumed that the two hats have around the same width h, so the blocked area is equal in both planes.

The total directivity of the antenna by taking into consideration the blockage will be the directivity of the aperture area that is calculated in the previous section minus the directivity from the area which it is blocked. The directivity of the small common area in the center should be added, because it will be subtracted twice in equation (3.17).

$$D = \frac{4\pi |G_a - 2G_b + G_c|^2_{max}}{P_a - 2P_b + P_c} \tag{3.17}$$

where

$$G_a \sim \pi \rho_\alpha^2 erf^2(\frac{d}{2\rho_\alpha})$$

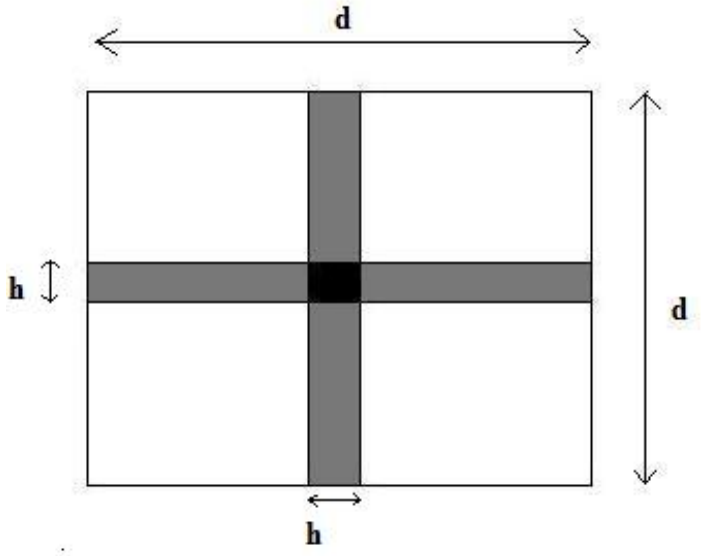

Figure 3.11: Blockage in the cylindrical reflector

$$G_b \sim E_{ay}(k\boldsymbol{x}\boldsymbol{r}, k\boldsymbol{y}\boldsymbol{r})_{max} = A(k\boldsymbol{x}, \boldsymbol{r})B(k\boldsymbol{y}, \boldsymbol{r}) =$$

$$= \int_{-d/2}^{d/2}\int_{-h/2}^{h/2} e^{-(\frac{x}{\rho_\alpha})^2} e^{-(\frac{y}{\rho_\alpha})^2}\,\mathrm{d}x\mathrm{d}y = \pi\rho_\alpha^2 erf(\frac{d}{2\rho_\alpha})erf(\frac{h}{2\rho_\alpha})$$

$$G_c \sim A(k\boldsymbol{x}, \boldsymbol{r})B(k\boldsymbol{y}, \boldsymbol{r}) = \int_{-h/2}^{h/2}\int_{-h/2}^{h/2} e^{-(\frac{h}{\rho_\alpha})^2} e^{-(\frac{y}{\rho_\alpha})^2}\,\mathrm{d}x\mathrm{d}y = \pi\rho_\alpha^2 erf^2(\frac{h}{2\rho_\alpha})$$

In a similar way the power of each aperture area is calculated and it is found to be

$$P_a = \frac{\pi}{2}\rho_\alpha^2 erf^2(\frac{\sqrt{2}d}{2\rho_\alpha})$$

$$P_b = \frac{\pi}{2}\rho_\alpha^2 erf(\frac{\sqrt{2}d}{2\rho_\alpha})erf(\frac{\sqrt{2}h}{2\rho_\alpha})$$

$$P_c = \frac{\pi}{2}\rho_\alpha^2 erf^2(\frac{\sqrt{2}h}{2\rho_\alpha})$$

Therefore, the total directivity of the aperture by taking into consideration the blockage is calculated by equation (3.17) and the result is:

$$D_b = \frac{4\pi}{\lambda^2}\frac{|\pi\rho_\alpha^2 erf^2(\frac{d}{2\rho_\alpha}) - 2\pi\rho_\alpha^2 erf(\frac{d}{2\rho_\alpha})erf(\frac{h}{2\rho_\alpha}) + \pi\rho_\alpha^2 erf^2(\frac{h}{2\rho_\alpha})|^2}{\frac{\pi}{2}\rho_\alpha^2 erf^2(\frac{\sqrt{2}d}{2\rho_\alpha}) - 2\frac{\pi}{2}\rho_\alpha^2 erf(\frac{\sqrt{2}d}{2\rho_\alpha})erf(\frac{\sqrt{2}h}{2\rho_\alpha}) + \frac{\pi}{2}\rho_\alpha^2 erf^2(\frac{\sqrt{2}h}{2\rho_\alpha})} \Leftrightarrow$$

$$D_b = \frac{8\pi^2\rho_\alpha^2}{\lambda^2}\frac{|erf(\frac{d}{2\rho_\alpha}) - erf(\frac{h}{2\rho_\alpha})|^4}{(erf(\frac{\sqrt{2}d}{2\rho_\alpha}) - erf(\frac{\sqrt{2}h}{2\rho_\alpha}))^2}$$

Figure 3.10 shows the directivity including blockage values for different frequencies, for a hat diameter h that is 10 times less than the reflector diameter d. The blockage loss for this case is calculated as $e_b = \frac{D_b}{D} = 0.84 = -0.78$ dB, which is higher than in the case of the circular parabolic reflector and this causes quite high sidelobes to the final radiation pattern of the antenna.

Finally, the far - field function of the rectangular aperture and that of the blockage aperture are plotted together in figure 3.12. The blockage is so small that its far-field is similar to a uniform aperture distribution. The total contribution of the blockage to the theoretical radiation pattern of the cylindrical reflector is shown in figure 3.13. The ETSI class 3 sidelobe level is also plotted in both figures, as well.

The rest of the subefficiencies of the cylindrical reflector are calculated by equations from [40] and they are also presented below in equations (3.18) - (3.19), where from $\theta_1 - \theta_2$ is the subtended angle of the cylindrical reflector and d is the diameter of the reflector

The spillover efficiency is

$$e_{sp} = \frac{\int_{\theta_1}^{\theta_2}|G(\theta)|^2\,\mathrm{d}\theta}{\int_0^{2\pi}|G(\theta)|^2\,\mathrm{d}\theta} \tag{3.18}$$

The illumination efficiency is

$$e_{ill} = \frac{F\int_{\theta_1}^{\theta_2}|G(\theta)|\frac{1}{cos(\theta/2)}\,\mathrm{d}\theta}{d\int_{\theta_1}^{\theta_2}|G(\theta)|^2\,\mathrm{d}\theta} \tag{3.19}$$

and the phase efficiency is

$$e_\phi = \frac{|\int_{\theta_1}^{\theta_2}G(\theta)\frac{1}{cos(\theta/2)}\,\mathrm{d}\theta|^2}{[\int_{\theta_1}^{\theta_2}|G(\theta)|\frac{1}{cos(\theta/2)}\,\mathrm{d}\theta]^2} \tag{3.20}$$

3.3 Antenna design parameters and phase center calculations for both antennas

The dimensions of both antennas and the theoretical directivity as well as the sub efficiencies that were determined from theory are found in table 3.1 for the circular parabolic reflector and in table 3.2 for the cylindrical reflector.

The only sub efficiency of a reflector antenna that depends on the localization of the phase reference point of the feed and requires the focal point to be at the phase center is the phase efficiency. The phase center should be calculated so that the phase efficiency can be maximized as much as possible.

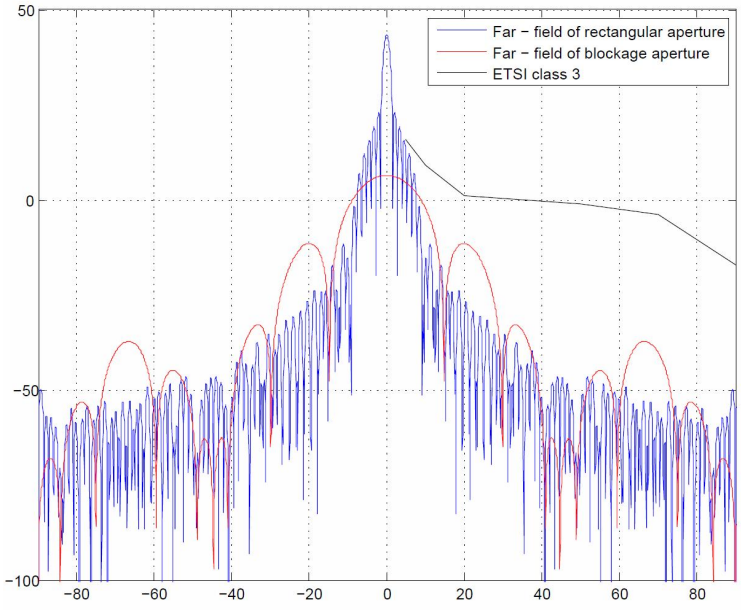

Figure 3.12: Radiation patterns of the rectangular aperture without blockage and the aperture that is blocked

When the phase reference point is moved, the phase of the far - field function changes as in equation (3.21).

$$G'(\theta,\phi) = G(\theta,\phi)e^{-jkr_0\mathbf{r}} \tag{3.21}$$

where, $\mathbf{r} = sin\theta cos\phi\boldsymbol{x} + sin\theta sin\phi\mathbf{y} + cos\theta\mathbf{z}$ and $r_0 = x_0\mathbf{x} + y_0\mathbf{y} + z_0\mathbf{z}$. If for example the antenna is located in the xy-plane, then z = 0 and $\theta = 90°$ and the phase is shown in equation 3.22:

$$phase = -kr_0\mathbf{r} = -k(x_0\mathbf{x} + y_0\mathbf{y})(cos\phi\mathbf{x} + sin\phi\mathbf{y}) = -k(cos\phi x_0 + sin\phi y_0) \tag{3.22}$$

Then, in order to maximize the phase efficiency, equation 3.23 is formed.

$$-k(cos\phi x_0 + sin\phi y_0) + \angle G(\frac{\pi}{2},\phi) = 0 \Leftrightarrow \angle G(\frac{\pi}{2},\phi) = k(cos\phi x_0 + sin\phi y_0) \tag{3.23}$$

In the next step, both parts of equation 3.23 are integrated and multiplied by $cos\phi$ as it is shown in equation 3.24 and by $sin\phi$ in equation 3.25.

$$\alpha = \int_0^{\theta_0} \angle G(\frac{\pi}{2},\phi)cos\phi\,\mathrm{d}\phi = k(x_0\int_0^{\theta_0} cos^2\phi\,\mathrm{d}\phi + y_0\int_0^{\theta_0} sin\phi cos\phi\,\mathrm{d}\phi) \tag{3.24}$$

$$\beta = \int_0^{\theta_0} \angle G(\frac{\pi}{2},\phi)sin\phi\,\mathrm{d}\phi = k(x_0\int_0^{\theta_0} cos\phi sin\phi\,\mathrm{d}\phi + y_0\int_0^{\theta_0} sin^2\phi\,\mathrm{d}\phi) \tag{3.25}$$

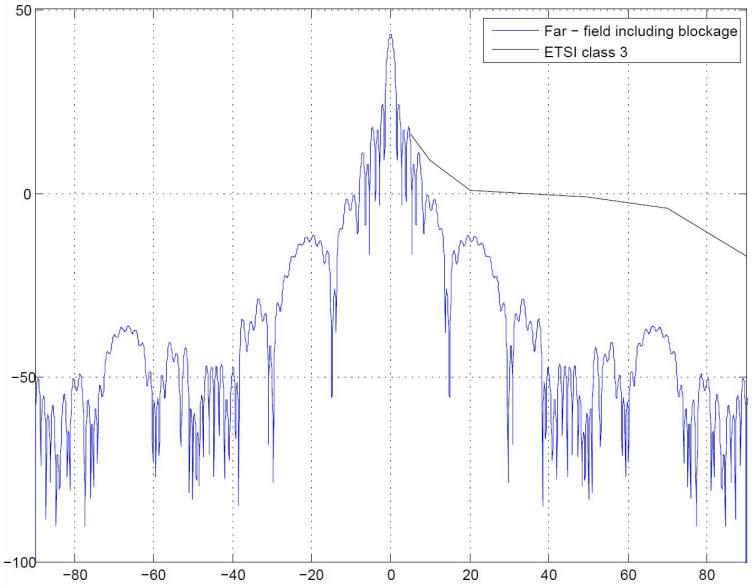

Figure 3.13: The radiation pattern of the cylindrical reflector including blockage

From 3.24 and 3.25 the maxtrix in 3.26 is created.

$$\begin{bmatrix}\alpha\\ \beta\end{bmatrix} = k\begin{bmatrix}\int_0^{\theta_0} cos^2\phi\,\mathrm{d}\phi & \int_0^{\theta_0} sin\phi cos\phi\,\mathrm{d}\phi\\ \int_0^{\theta_0} cos\phi sin\phi\,\mathrm{d}\phi & \int_0^{\theta_0} sin^2\phi\,\mathrm{d}\phi\end{bmatrix}\begin{bmatrix}x_0\\ y_0\end{bmatrix} \tag{3.26}$$

The values of x_0 and y_0 that satisfy equation 3.26 , are the coordinates of the phase center and the phase efficiency should be calculated, only when the feed is located at its phase center.

Another way of calculating the phase center of rotational symmetric reflectors, illuminated by a hat feed is to use equation 7 from [41], which is shown in equation (3.27). The phase center of the hat is defined to be ring-shaped and the 45° co - polar far -field function is used to calculate the maximum phase efficiency, which will contribute to a maximum aperture efficiency [42].

$$e_\phi = \frac{1}{I_w^2}\left|\int_0^{\theta_0} w(\theta)e^{j[\phi(\theta)-kz_0cos\theta-k\rho_0sin\theta(1+cos\theta)]}\,\mathrm{d}\theta\right|^2 \tag{3.27}$$

where
θ_0 is the subtended half angle
$w(\theta) = |G_{co45}(\theta)|tan(\theta/2)$
$\phi(\theta)$ is the phase of $G_{co45}(\theta)$
and $I_w = \int_0^{\theta_0} w(\theta)\,\mathrm{d}\theta$
z_0 and ρ_0 are the coordinates of the phase center in yz or xz planes.

Parameter	**Value**
Diameter (d)	190 mm
Focus (F)	36.5 mm
Half subtended angle (θ_0)	105°
Depth of focus (Δz)	61.9 mm
Directivity D_0 without taper (at 71 GHz)	43 dBi
Theoretical feed loss	-1.7 dB ($e_{ap} = 0.68$)
Theoretical spillover loss	-0.3 dB ($e_{sp} = 0.93$)
Theoretical blockage loss	-0.15 dB ($e_b = 0.96$)
Directivity D (at 71 GHz)	41.3 dBi

Table 3.1: Circular parabolic reflector

Parameter	**Value**
Length, width (d)	168.4 mm
Focus (F)	32.3 mm
Subtended angle (θ_0)	105°
Depth of focus (Δz)	54.85 mm
Directivity D_0 without taper (at 71 GHz)	43 dBi
Directivity of 10 dB taper D_t (at 71 GHz)	42.3 dBi
Theoretical blockage loss	-0.78 dB ($e_b = 0.84$)
Directivity D (at 71 GHz)	41.52 dBi

Table 3.2: Cylindrical reflector

In general, the focal point of the reflector should be located at the phace center of the feed, in order to maximize the directivity and achieve low sidelobes. Therefore, it is very important to calculate the phase center correctly from the feed, before designing the complete reflector.

4

Detailed designs and simulation results

4.1 Electromagnetic field simulation software

The two antenna designs that were presented in the previous section are simulated in two different softwares, HFSS and G2DMULT. HFSS is a 3D commercial simulation tool for full wave electromagnetic field simulation using the finite element method (FEM) [43] and G2DMULT is a 2D Chalmers internal simulation tool implemented in Fortran, which uses the moment method (MOM) [44], [45], [46], [47], [48], [49], [50], [51], [52], [53].

Only the hat feed of the circular reflector is simulated in HFSS, because it is impossible to simulate the complete design due to computer memory limitations. Moreover, both of the reflectors and their feeds that consist the cylindrical reflector, that is illuminated by a parallel plate are simulated in G2DMULT.

There was an attempt to simulate the complete circular reflector in G2DMULT as well, but the problem is not two dimensional and the results are not considered to be accurate, since G2DMULT is a 2D solver and it takes into consideration the currents that exist in E and H plane only. In a rotational symmetric design there are currents in the other planes as well and they cannot be neglected.

4.2 Circular reflector

The feed of the circular reflector is designed and simulated in HFSS and the total radiation pattern, as well as the directivity are plotted and calculated in MATLAB by applying the equations from chapters 7 and 9 of [39] for rotational symmetric antennas.

4.2.1 Design and simulations of the hat feed

The parabolic reflector is illuminated by a self supported hat feed on top of the axial located circular waveguide in order to achieve low sidelobe level and reduce the blockage efficiency [54]. Moreover, a hat - feed has low cross polarization, is wideband and has low ohmic losses [55], [56], [57], [58], [59].

The hat is illuminated by a circular waveguide, whose diameter needs to be selected, so that all the wavelengths of E - band (71 - 86 GHz) can propagate through and no higher order modes. From [60], the different diameter sizes do not cover the entire E-band, therefore, the radius is defined so that the first and second cut - off frequencies of the TE - modes are far away than the desired frequencies. Inside the waveguide only the dominant mode TE_{11} will propagate and the cut - off frequency of the first and the second TE modes are calculated by equation (4.1) from [61].

$$\lambda_{c11} = \frac{2\pi a}{p_{11}}, \lambda_{c21} = \frac{2\pi a}{p_{21}} \tag{4.1}$$

where $p_{11} = 1.841$ and $p_{21} = 3.054$

For a = 1.5 mm, $f_{c11} = 58.8$ GHz and $f_{c21} = 97.2$ GHz, therefore an inner diameter of 3 mm is selected for the circular waveguide.

The distance of the hat from the circular waveguide is selected to be equal with the radius of the waveguide, which is 1.5 mm. Moreover, the hat is designed to have corrugations, in order to reduce the cross polar level and the spillover loss. The hat is designed to have three corrugations whose depth should be $\lambda/4$ [62], [63], [64], [65].

A sketch of the cross section of the hat design with all the dimensions in mm is presented in figure 4.1. The diameter of the hat is around 4λ for the center wavelength and it is almost 11 times less than the diameter of the circular parabolic reflector.

A dielectric plug needs to be placed between the hat and the waveguide to support the hat. In this case teflon is selected with $\epsilon_r = 2.1$, in order to let the electromagnetic wave propagate through it and absorb as little as possible. The thickness of the dielectric material should be $\frac{\lambda}{2\sqrt{\epsilon_r}}$. A 3D image of the hat feed without the dielectric included can be shown in figure 4.2.

An image of the cross section of the hat feed with the dielectric support is shown in figure 4.3.

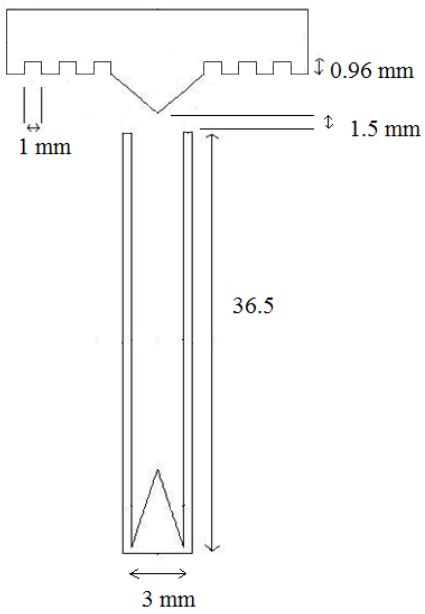

Figure 4.1: Circular reflector corrugated hat feed cross section

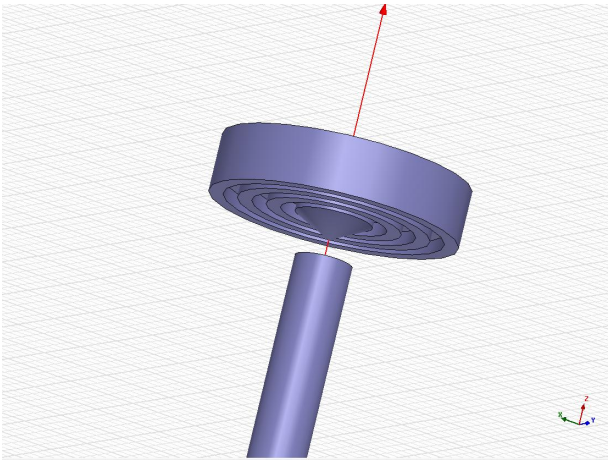

Figure 4.2: Circular reflector corrugated hat feed

4.2.2 Sub efficiencies and total aperture efficiency calculation

The different sub efficiencies that are contributing to the total aperture efficiency are the blockage efficiency, that depends on the hat diameter, the spillover efficiency, the illumination efficiency, the sidelobe polarization efficiency and the phase efficiency. All the equations for calculating the sub efficiencies are found in chapter 9 at [39] and the

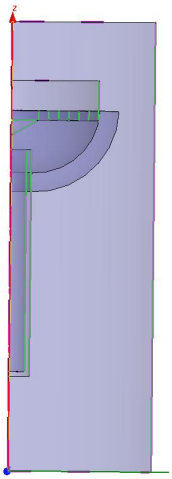

Figure 4.3: Cross section of the corrugated hat feed with the dielectric support

results depend on the co - polar and cross - polar far - field functions of the 45° plane.

The real and the imaginary part of the complex E-field are extracted from HFSS for E and H plane respectively. In this case the polarization is along the y-axis and the antenna is along the z-axis, therefore E-plane is the yz plane, $\phi = 90°$ and the H-plane is the xz plane, $\phi = 0°$. The co-polar and cross-polar of the 45° plane can be constructed by using equation 4.2.

$$G_{co45} = \frac{1}{2}[G_E + G_H] \tag{4.2}$$

$$G_{xp45} = \frac{1}{2}[G_E - G_H]$$

After calculating the subefficiencies, it is noticed that the illumination efficiency is relatively low and this is due to the fact that the taper of the hat is more than 10 dB in all planes. In order to improve the illumination loss and achieve a taper of around 10 dB, one corrugation is removed and the new hat shape is shown in figure 4.4.

The radiation patterns of the feed for E and H planes are plotted in figures 4.5 and 4.6 respectively, for some of the frequencies in the E-band. A variation is noticed in the E and H planes for different frequencies, which is quite normal to expect.

Moreover, the values of all sub efficiencies for the center frequency of 78.5 GHz are presented in table 4.1. The spillover efficiency and the blockage efficiency are similar to the theoretical values that were calculated in the previous chapter and were presented in table 3.1. The polarization sidelobe efficiency is low, as well as the illumination efficiency, because the hat feed is not optimized.

An optimization of the hat feed would increase these subeffieciencies and the total aperture efficiency would be higher. The phase efficiency is calculated from the equations in [41] and the phase center is assumed to have a ring shape.

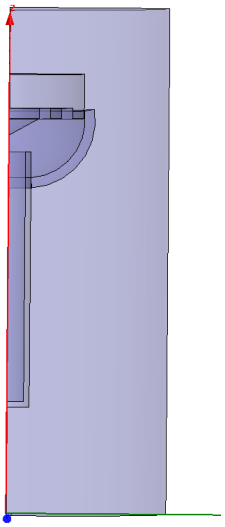

Figure 4.4: Cross section of the modified corrugated hat feed with dielectric support and two corrugations

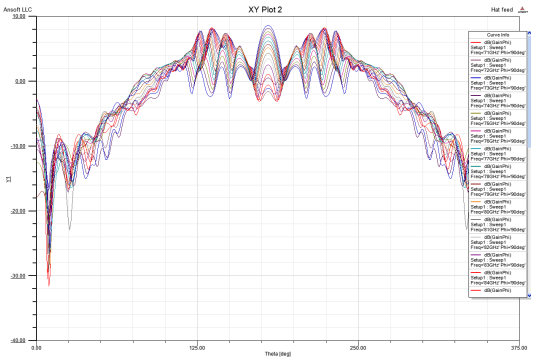

Figure 4.5: E-plane radiation pattern of the circular hat feed for some of the frequencies calculated in HFSS

The calculation of the coordinates of the phase center depends only on the complex E - field of the 45° plane. Due to the significant difference in the radiation patterns of E and H planes, the phase center would be different for each one of them. This results to a phase error in the final radiation patterns of the complete circular reflector.

4.2.3 Total directivity and radiation patterns of the circular reflector

The complete reflector design could not be simulated in HFSS, thus the aperture field and the far-field function of the reflector are calculated analytically from the equations of [39]. The antenna is considered to be rotationally symmetric and the equations are

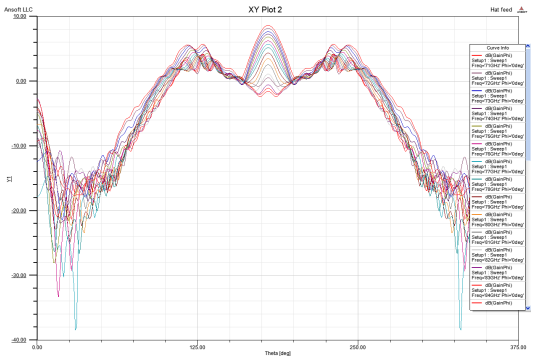

Figure 4.6: H-plane radiation pattern of the circular hat feed for some of the frequencies calculated in HFSS

Type	Value
Spillover efficiency (e_{sp})	0.95
Illumination efficiency (e_{ill})	0.66
Polarization efficiency (e_{pol})	0.805
Phase efficiency (e_{ph})	0.98
Blockage efficiency (e_b)	0.98
Total aperture efficiency (e_{ap})	0.49 (-3.1 dB loss)

Table 4.1: Total aperture efficiency of the circular reflector for f = 78.5 GHz

valid, assuming to have a perfect paraboloid with no surface errors. The total directivity of the circular reflector is calculated by equation (3.15) and the results vary for different wavelengths.

For the center frequency the directivity is D = 39.9 dBi and the radiation patterns are shown in figures 4.7, 4.8 and 4.9 for E, H and 45° planes, respectively. The ETSI class 3 sidelobe level requirement is fulfilled for all the cases.

As it was mentioned before, the difference in the radiation patterns of E and H planes of the feed leads to phase errors in the final radiation patterns of the reflector, as well as reduced directivity. Assuming the case of having no phase errors at all, the directivity of the circular reflector would be D = 42.4 dBi. The radiation patterns are also different and the results are plotted in figures 4.10 , 4.11 and 4.12.

In that case the ETSI class 3 sidelobe level is fulfilled for all the planes, too and the beamwidth of the E and H planes is similar to the one of the 45° plane. The difference of 2.5 dB in directivity, between the two cases is due to the phase errors, despite that the

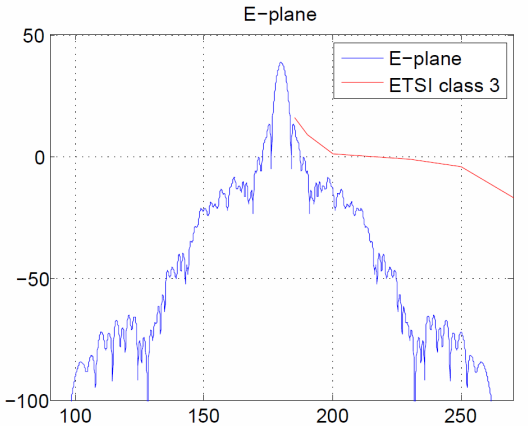

Figure 4.7: E-plane radiation pattern of the circular reflector for f = 78.5GHz

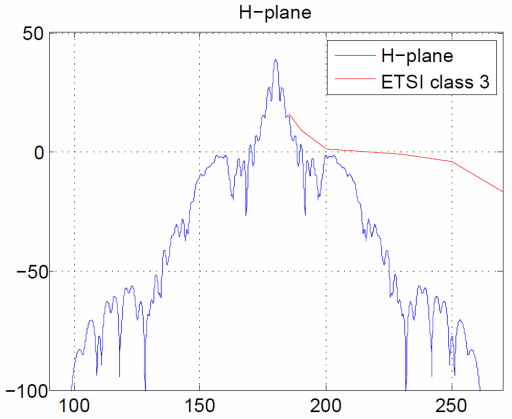

Figure 4.8: H-plane radiation pattern of the circular reflector for f = 78.5GHz

phase efficiency is close to 1. The non similarity of the symmetry planes is something that needs to be improved. Therefore, one of the main optimization cost function in hat feed designs is to try to achieve similar radiation patterns in the E and H planes.

Finally, it is noticed that the only plane that has small phase errors is the 45° plane, from which the phase center is calculated. This is a proof that the phase reference point is at the phase center of the feed.

The variation of the radiation patterns of the circular reflector for all the frequencies in the E-band is shown in figures 4.13, 4.14 and 4.15 for 45°, E and H planes respectivelly. It is noticed that there is not a big variation in the radiation patterns, which means that the design of the circular reflector antenna is broadband.

The directivity of 39.9 dBi in the center frequency is above the gain requirements and assuming that in the simulations the material of the antenna is perfect electric conductor,

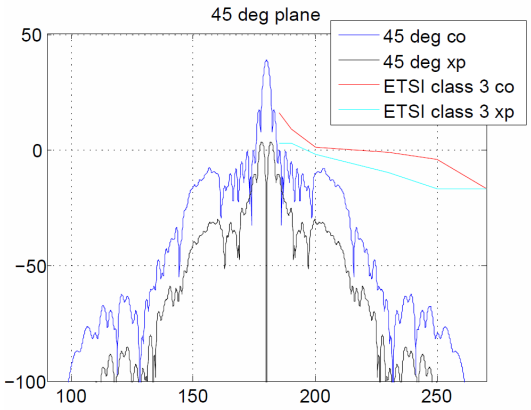

Figure 4.9: 45°-plane radiation pattern of the circular reflector for f = 78.5GHz

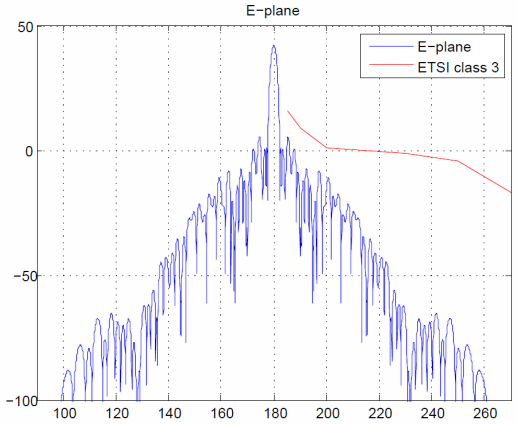

Figure 4.10: E-plane radiation pattern of the circular reflector without phase errors for f = 78.5GHz

in reality there will be more losses to be added. Thus, the final gain would be around 39.4 dBi, for radiation losses of 0.5 dB.

The directivity of the circular reflector for the frequencies in the E-band is shown in figure 4.16. Moreover, the aperture efficiency is different for different frequencies and this is due to the difference in the subefficiencies. In figure 4.16, the loss in the theoretical directivity that its subefficiency causes is shown, as well.

It is noticed that the calculated directivity is not similar to the directivity result if all the sub efficiencies are subtracted from the theoretical directivity of a uniform aperture. The reason of that is the high sidelobes that are noticed in the lower frequencies of the E-band, due to high cross polar level in these frequencies.

Another requirement of the project is that the return loss should be higher or equal than 10 dB. In figure 4.17, that is taken from HFSS it is noticed that the return loss

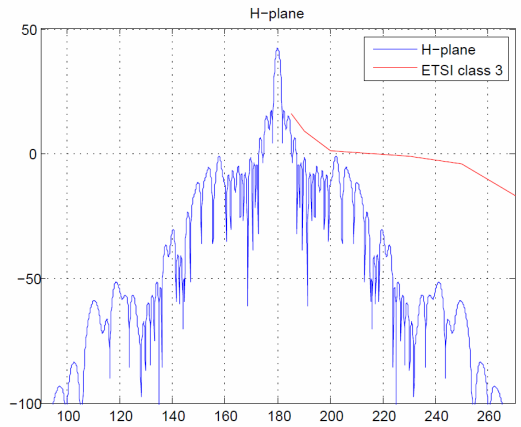

Figure 4.11: H-plane radiation pattern of the circular reflector without phase errors for f = 78.5GHz

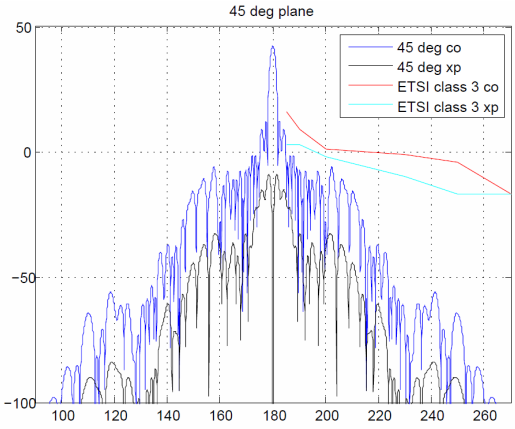

Figure 4.12: 45°-plane radiation pattern of the circular reflector without phase errors for f = 78.5GHz

fulfills the requirements of the project for almost all of the frequencies in the E-band.

4.2.4 Directivity and radiation patterns of the circular reflector with no radome in the hat feed

The results that have just been presented correspond to the radiation patterns of the circular reflector, when radome is included in the hat feed, which a realistic approach of the antenna design. Simulating the case when no radome is included, it is noticed that the directivity is higher and it is equal with D = 39.9 dBi, for the center frequency of 78.5 GHz.

Assuming no phase errors the directivity for the center frequency is D = 42.4 dBi

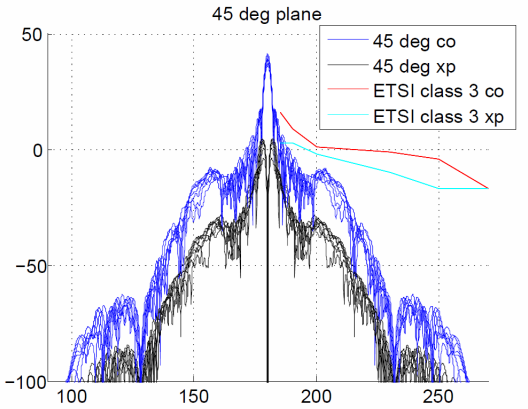

Figure 4.13: 45°-plane radiation pattern variation for some of the frequencies in the E-band

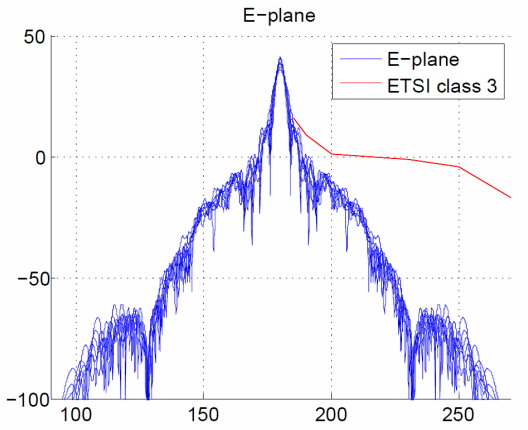

Figure 4.14: E-plane radiation pattern variation for some of the frequencies in the E-band

and this value is similar to the previous case when radome included and the phase errors are neglected, as well. The radiation patterns are not plotted, but they are almost the same with the ones in figures 4.10 - 4.12.

Firstly, the radiation patterns of the hat feed with no radome are shown in figures 4.18 and 4.19 for E and H plane respectively.

Then, the radiation patterns for the center frequency of the complete circular reflector antenna when no radome is included in the feed, are shown in figures 4.20, 4.21 and 4.22 for E, H and 45° planes respectively.

Finally, the radiation patterns for 6 different frequencies in the E-band (71, 74, 77, 80, 81 and 86 GHz) are plotted together in the same plot for E, H and 45° planes in figures 4.23, 4.24 and 4.25 respectively. It is noticed that there is no big variation between the radiation patterns, as in the previous case when teflon was included in the feed.

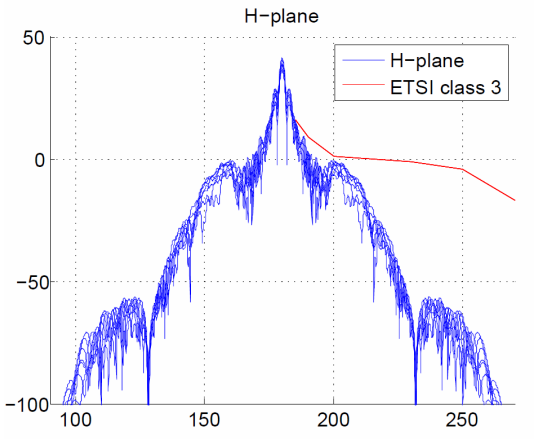

Figure 4.15: H-plane radiation pattern variation for some of the frequencies in the E-band

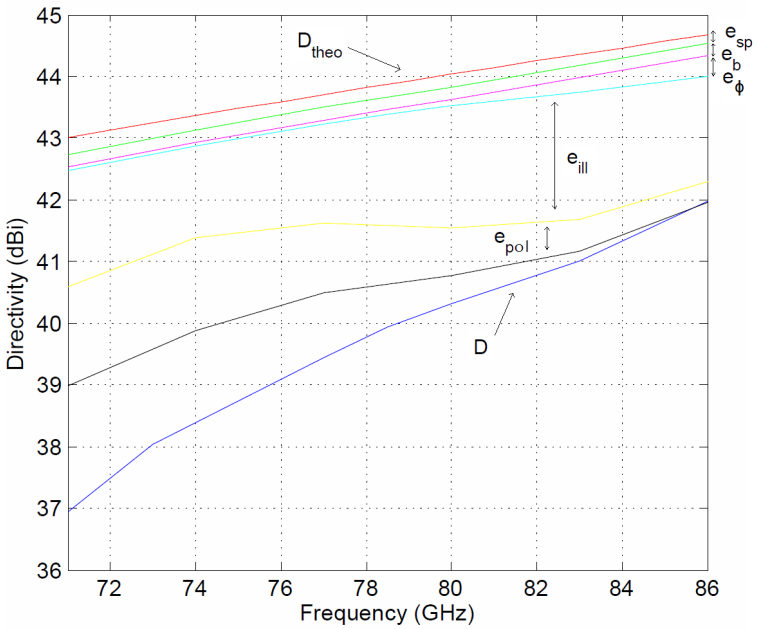

Figure 4.16: Directivity and aperture efficiency towards frequency

Therefore, the main conclusion is that when radome is included in the hat feed the directivity is lower than having no radome at all. Of course, radome is mandatory to exist in the feed in order to hold the waveguide and the hat in place. The shape of the radiation pattern of the circular reflector does not seem to change significantly with the existence or not of radome, however, the variation with frequency in the radiation pattern of the feed for E and H plane, seems to get affected by the existence of radome.

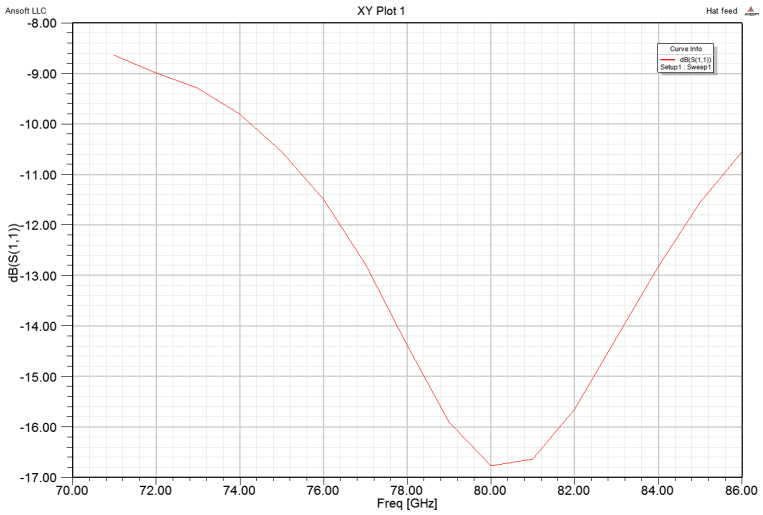

Figure 4.17: Reflection coefficient of the circular hat feed in the E-band

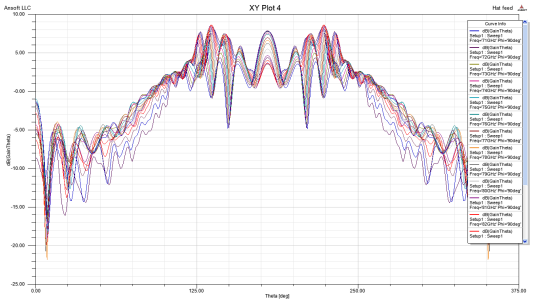

Figure 4.18: E-plane radiation pattern of the hat feed without radome for all the frequencies in the E-band

Finally, the polarization sidelobe efficiency is better in the case when radome is not included.

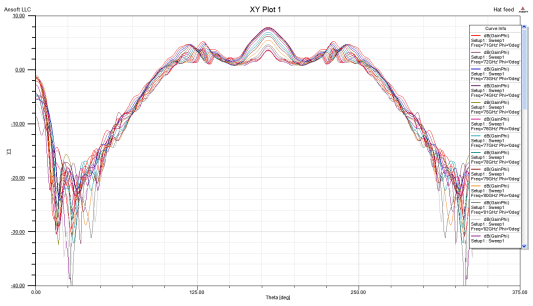

Figure 4.19: H-plane radiation pattern of the hat feed without radome for all the frequencies in the E-band

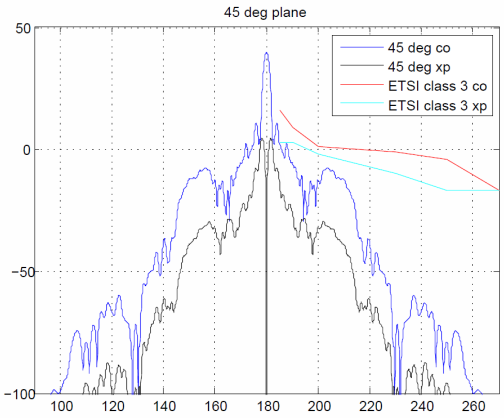

Figure 4.20: 45°-plane radiation pattern of the circular reflector for f = 78.5 GHz, with no radome in the feed

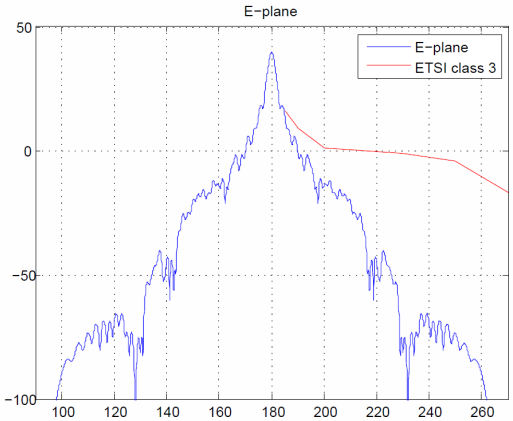

Figure 4.21: E-plane radiation pattern of the circular reflector for f = 78.5 GHz, with no radome in the feed

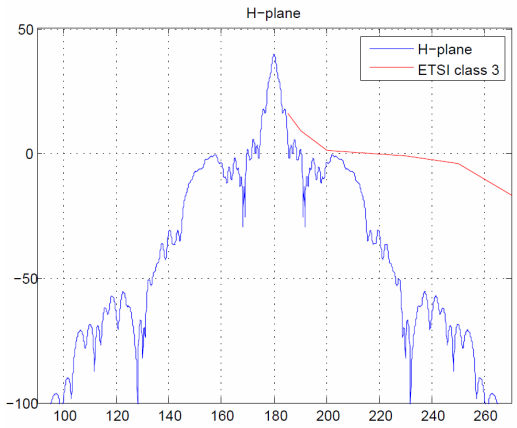

Figure 4.22: H-plane radiation pattern of the circular reflector for f = 78.5 GHz, with no radome in the feed

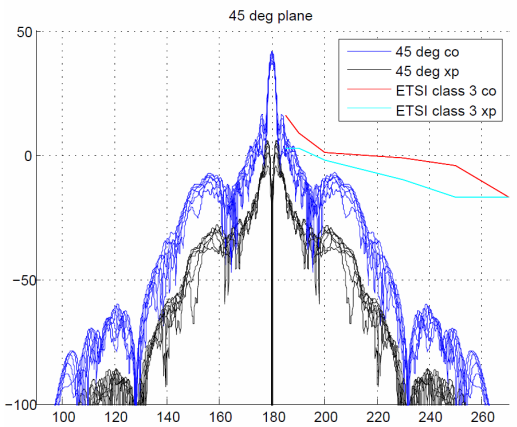

Figure 4.23: 45°-plane radiation pattern of the circular reflector for f = 71-86 GHz with no radome in the feed

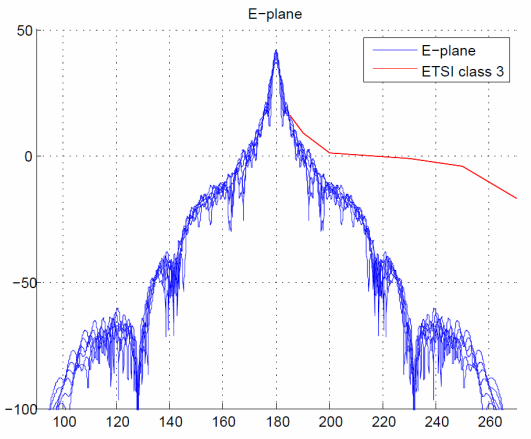

Figure 4.24: E-plane radiation pattern of the circular reflector for f = 71-86 GHz with no radome in the feed

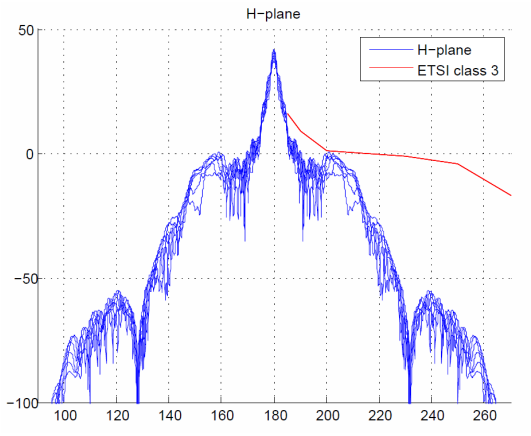

Figure 4.25: H-plane radiation pattern of the circular reflector for f = 71-86 GHz with no radome in the feed

4.3 Cylindrical reflector

The cylindrical reflector with a square aperture is considered to be a two dimensional design, so it can be successfully implemented in G2DMULT, assuming that the third dimension is infinite long. The design is consisted of two parabolic reflectors that are illuminated by hat feed structures. Firstly, the hat feeds of both reflectors are designed and simulated and then the complete reflector structure is added. The directivity is calculated to be the sum of the directivities from both reflectors separately.

G2DMULT is a program developed in the programming language Fortran and an antenna structure is designed by uniting several nodes, which are defined in a two dimensional coordinate system. Due to the fact that the interface of G2DMULT is not so user friendly, programming in MATLAB is done in order to insert these nodes in the .txt files that are read by G2DMULT.

In general, MATLAB is used not only to design the antenna, but also to execute G2DMULT and plot the results from the radiation patterns, too. The complex E - field of all radiation patterns is exported from G2DMULT to MATLAB and this is used to plot the amplitude and the phase of the far -field functions of the antennas that are designed.

Finally, the optimization procedure of the hat feeds is done by an algorithm called GODLIKE that has been programmed in MATLAB. In that case MATLAB is calling G2DMULT several times and this procedure might last around 24 hours, depending on the number of iterations. Therefore, G2DMULT is connected with MATLAB in all steps of design, simulation and optimization.

4.3.1 Hat feed inside parallel plate structure

The hat feed inside the parallel plate structure is illuminated by a WR-12 rectangular waveguide, that is working in the band of 60 - 90 GHz [66]. The dimensions of the rectangular waveguide are a = 3.099 mm and b = 1.549 mm. The width of the parallel plate structure is mainly determined by dimension b of the waveguide together with the thickness of the metal.

The hat that is illuminated by the waveguide does not need any dielectric support, because it is already supported by the parallel plates. The waveguide is propagating with the dominant TE_{10} mode and the distance between the hat and the waveguide should be equal with size a of the waveguide, in order for the wavelengths to avoid to be in the cut off. A schematic of the hat feed is shown in figure 4.26.

All the dimensions of the design in G2DMULT are given in wavelengths and the design is done for the center wavelength of the frequency of 78.5 GHz. Moreover, in G2DMULT the waveguide is excited in the center, therefore an absorber is used as it can be noticed in figure 4.26, in order to avoid reflections from the bottom of the waveguide. The length of the absorber is 0.2 times the length of the waveguide.

Assuming that the coordinate system in figure 4.26 is the xy-plane and the hat is located along y-axis, the excitation is along z-axis. Firstly, the radiation pattern of the waveguide without the hat is plotted in figure 4.27 and then the radiation pattern of

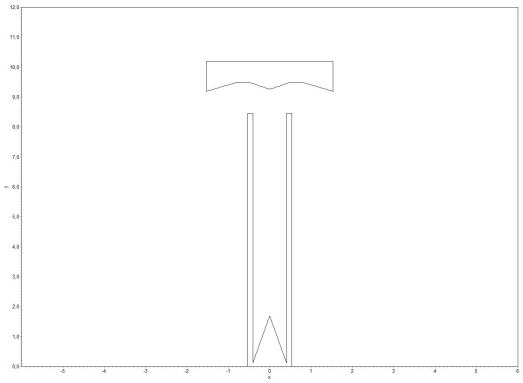

Figure 4.26: Hat feed inside parallel plate (dimensions normalizes to the wavelength at 78.5 GHz)

the waveguide and the hat is shown in figure 4.28. It should be noticed that the hat is pointing downwards, therefore in that case the beam is centered at $-90°$ and the half subtended angle is from $-90°$ to $15°$ and from $165°$ to $270°$ in figure 4.28.

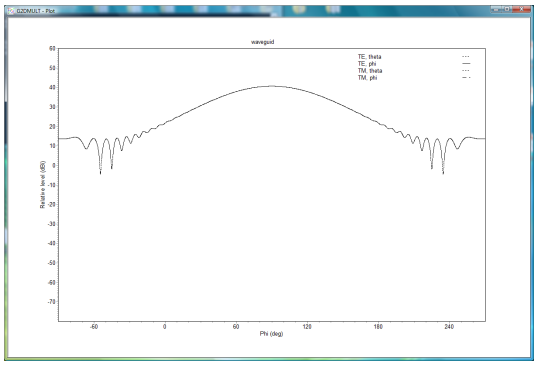

Figure 4.27: Radiation pattern of the open waveguide calculated in G2DMULT

The radiation pattern of the hat feed for all the frequencies in the E-band with a frequency step of 1 GHz, i shown in figure 4.29. As it can be seen, there is not much variation in the radiation pattern for different frequencies. However, the final shape of the hat is a result of the optimization procedure that will be further analyzed in the sections below.

4.3.2 Corrugated hat feed, fed by the parallel plate

The corrugated reflector, or the corrugated hat feed, which is illuminated by the parallel plate aperture is also designed in G2DMULT, since it is assumed to be a two dimensional problem as well. This corrugated hat does not need dielectric support, because it can be

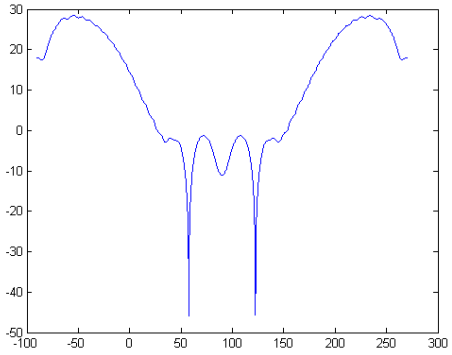

Figure 4.28: Radiation pattern of the hat feed calculated in G2DMULT

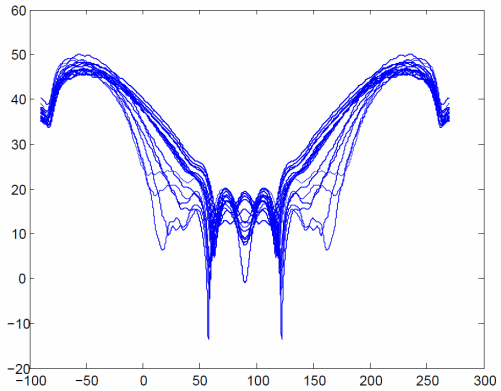

Figure 4.29: Radiation pattern of the hat feed plotted in G2DMULT for some of the frequencies in the E-band

supported by metal in the center of the aperture, where there is already blockage from the previous hat feed, and on the edges of the parallel plate aperture. A design of the corrugated hat feed in G2DMULT is shown in figure 4.30.

This hat is designed to have corrugations, in order reduce the spillover efficiency and achieve low sidelobes in the final radiation pattern. The depth of the corrugations should be $\lambda/4$ and it is decided to have 3 corrugations on each side of the hat. The E - field is along the x dimension normal to the parallel plate.

The radiation pattern of the corrugated hat feed is shown in figure 4.31, with the beamwidth centered at $-90°$. As it was mentioned before, the excitation is along x-axis and the ripple that is noticed in the radiation pattern of the hat comes from the reflections of the low corner of the parallel plate. This can be proved by calculating the period of the ripple.

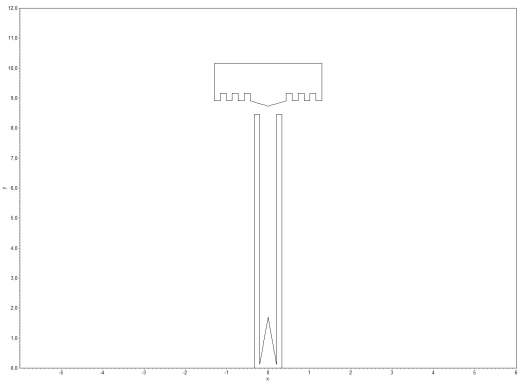

Figure 4.30: Cross section of linear corrugated hat feed (dimensions normalized to the wavelength at 78.5 GHz)

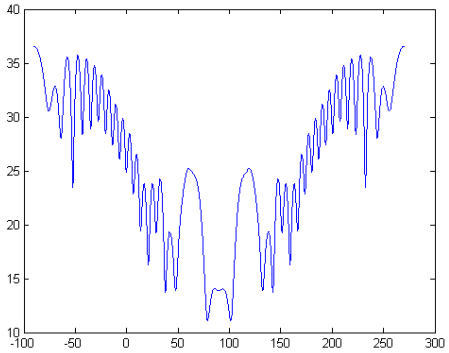

Figure 4.31: Radiation pattern of the corrugated hat feed calculated in G2DMULT

The difference between two maxima will give the distance of the reflection by equation (4.3).

$$d = \frac{\lambda}{sin\theta} \tag{4.3}$$

In that case the distance is equal with the length of the parallel plate, therefore the reflection occurs at the low edge of the parallel plate. Finally, the shape of the hat is optimized using GODLIKE, too.

4.3.3 Optimization of the hat feeds in GODLIKE

Both hat feeds are optimized by the algorithm called GODLIKE, which is programmed in MATLAB. The name GODLIKE comes from Global Optimum Determination by Linking and Interchanging Kindred Evaluators. The algorithms that are combined in

GODLIKE are GA (Genetic Algorithm), DE (Differential Evolution), ASA (Adaptive Security Algorithm) and PSO (Particle Swarm Optimization). The combination of these algorithms produces robustness, something that non of them could achieve individually [67].

The solutions of GODLIKE appear in a Pareto front among x and y axis, which correspond to the cost functions that are defined and then the user selects one solution from the Pareto front, which does not have to coincide exactly with the optimum point.

Three main cost functions are defined in GODLIKE for both hat feeds. The first cost has to do with the length of the hat, which should be as small as possible in order to improve the blockage efficiency. Furthermore, the radiation pattern of the hat, has to follow the 10 dB taper of the ideal Gaussian curve and finally, the phase efficiency should be maximized. The phase efficiency depends on the location of the phase reference point at the phase center.

The parameters that were tuned in GODLIKE optimization are different for the two hat feeds. For the hat feed structure that is located inside the parallel plate, the parameters that are tuned are the coordinates of the nodes that create the shape of the hat, while the position of the hat is determined to be in a distance a/2 on top of the waveguide, where a = 3.099 mm. In the case of the corrugated hat feed the length of the corrugations is optimized together with the the shape and the position of the hat.

The selected optimum hat designs and the radiation patterns that occur from them were presented in figures 4.26 and 4.31 in the previous sections.

The total aperture efficiency of the hat feeds and its sub efficiencies are calculated by the equations of [40]. The aperture efficiency is also called feed efficiency, because it is mainly depended on the hat feed. The results are shown in tables 4.2 and 4.3 for both hat feed designs.

Type	**Value**
Spillover efficiency (e_{sp})	0.998
Illumination efficiency (e_{ill})	0.794
Polarization efficiency (e_{pol})	1
Phase efficiency (e_{ϕ})	0.993

Table 4.2: Subefficiencies for parallel plate hat feed

4.3.4 Odd G2DMULT results for the corrugated hat feed reflector and HFSS simulations

In the case of the corrugated reflector, which is illuminated by the waveguide parallel plate, the polarization is along x-axis and the design is along xy axis. It was found

Type	Value
Spillover efficiency (e_{sp})	0.944
Illumination efficiency (e_{ill})	0.915
Polarization efficiency (e_{pol})	1
Phase efficiency (e_{ϕ})	0.879

Table 4.3: Subefficiencies for corrugated hat feed calculated by G2DMULT

that G2DMULT gives some numerical errors for that polarization. The excitation in G2DMULT is done in the center of the waveguide, which in that case is the parallel plate. In reality the result of the radiation pattern should not depend on the position of the excitation.

However, the radiation pattern in figure 4.31 changes when the position of the excitation is changed, something that is not physically correct. Therefore, for that case the optimum hat design from GODLIKE is selected and designed in HFSS as it is shown in figure 4.32.

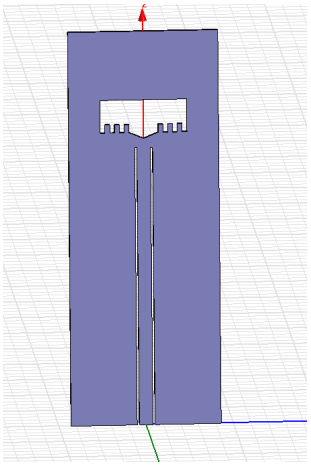

Figure 4.32: Corrugated hat designed in HFSS

The front and the back faces of the design are assumed to be perfect magnetic walls and the width is incremental small ($\lambda/10$) along x-axis. In that way, HFSS is considering the problem to be two dimensional and the simulation time is small, comparable with G2DMULT. The radiation pattern of the hat feed is shown in figure 4.33 and the difference between the radiation pattern of figure 4.31 is obvious.

The radiation pattern of the corrugated hat feed for all the frequencies in the E-band

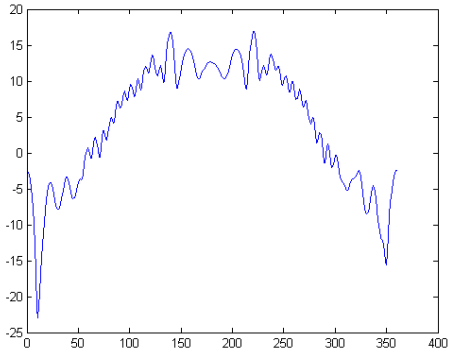

Figure 4.33: Radiation pattern of the corrugated hat feed calculated in HFSS

is shown in figure 4.34, which is taken from HFSS. It is noticed that the shape of the radiation pattern is the same, however, there is a difference in the amplitude due to the different frequencies.

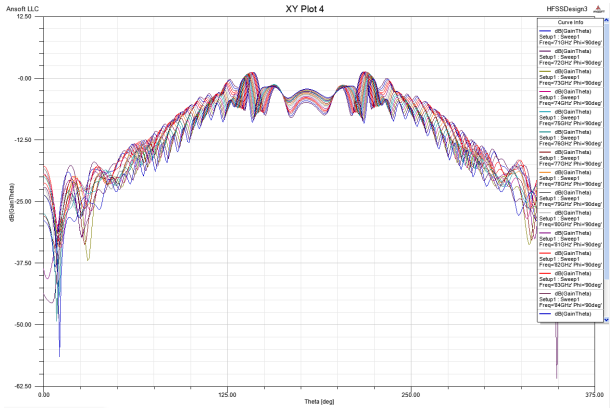

Figure 4.34: Radiation pattern of the corrugated hat feed calculated in HFSS for all the frequencies in the E-band

The new radiation pattern leads to different result in the aperture efficiency. The equations that calculate the sub efficiencies are not different, but the complex E-field is different in amplitude and phase. Therefore, the new sub efficiencies results are shown in table 4.4 for the corrugated hat feed.

4.3.5 Total aperture efficiency and directivity

In the previous sections the subefficiencies of each hat feed were calculated, but the general expression of the total aperture efficiency of the cylindrical reflector is $e_{ap} = e_t e_l$,

Type	Value
Spillover efficiency (e_{sp})	0.989
Illumination efficiency (e_{ill})	0.932
Polarization efficiency (e_{pol})	1
Phase efficiency (e_{ϕ})	0.96

Table 4.4: Subefficiencies for corrugated hat feed simulated in HFSS for f = 78.5 GHz

which is the result of the transverse aperture efficiency and the longitudinal aperture efficiency [40].

The transverse aperture efficiency is the aperture efficiency that results from the corrugated hat feed and it can be found on table 4.4. The longitudinal aperture efficiency comes from the one dimensional reflector inside the parallel plate and it is found on table 4.2.

At [40], it is shown that the illumination efficiency and the phase efficiency can become separable in the longitudinal and transverse direction. However, it has not been yet investigated whether the same can be assumed for the spillover efficiency. The polarization efficiency is 1 in both cases, therefore it does not contribute to the final aperture efficiency and the blockage efficiency has been already defined for both cases.

The total blockage efficiency depends on the length of the hat and it is found to be $e_b = 0.866$. The length of each hat is around 11 mm and equation 3.17 of chapter 3.2.2 is applied to estimate the blockage in two directions. The blockage efficiency is calculated, assuming a 10 dB of illumination taper. The illumination taper might be slightly different for different frequencies in the E-band, because the aperture field will be different, so the blockage efficiency will vary along frequency. However, the results are not estimated to be much different than assuming a constant blockage efficiency along the frequency range.

The total illumination efficiency is

$$e_{ill,tot} = e_{ill,t}e_{ill,l} = 0.794 * 0.932 = 0.74$$

from tables 4.2 and 4.4.

In the same way, the total phase efficiency is

$$e_{\phi,tot} = e_{\phi,t}e_{\phi,l} = 0.993 * 0.96 = 0.953$$

Assuming that the total spillover efficiency is the sum of the transverse spillover and the longitudinal spillover efficiencies, then

$$e_{sp,tot} = e_{sp,t}e_{sp,l} = 0.998 * 0.989 = 0.987$$

Therefore, the total aperture efficiency of the cylindrical reflector is

$$e_{ap,tot} = e_{sp,tot}e_{ill,tot}e_{\phi,tot}e_{b,tot}e_{pol,tot}$$

The result is shown in table 4.5, together with all the subefficiencies that contribute. The total aperture efficiency of the cylindrical reflector is calculated for the center frequency. Assuming that the radiation patterns of the feeds are not very different along the frequencies in the E-band, then it can be assumed that the total aperture efficiency is the same for 71 - 86 GHz.

Type	**Value**
Total spillover efficiency (e_{sp})	0.987
Total illumination efficiency (e_{ill})	0.74
Total Polarization efficiency (e_{pol})	1
Total Phase efficiency (e_{ϕ})	0.953
Total blockage efficiency (e_{b})	0.866
Total aperture efficiency (e_{ap})	0.603

Table 4.5: Total aperture efficiency of the cylindrical reflector for f = 78.5 GHz

The total directivity of the cylindrical reflector is the sum of the directivities from each reflector separately. The general expression of the directivity becomes separable in the different E and H planes of the antenna, as it is shown in equation (4.4).

$$D = \frac{4\pi U_{max}}{P_{rad}} = D_\theta D_\phi \tag{4.4}$$

where,

$$P_{rad} = \int_{-\pi}^{\pi}\int_{0}^{\pi} |E_\theta(\theta)|^2|E_\phi(\phi)|^2 sin\theta \,\mathrm{d}\theta\mathrm{d}\phi = \int_{0}^{\pi} |E_\theta(\theta)|^2 sin\theta \,\mathrm{d}\theta \int_{-\pi}^{\pi} |E_\phi(\phi)|^2 \,\mathrm{d}\phi$$

and

$$P_\theta = \int_{0}^{\pi} |E_\theta(\theta)|^2 sin\theta \,\mathrm{d}\theta$$

$$P_\phi = \int_{-\pi}^{\pi} |E_\phi(\phi)|^2 \,\mathrm{d}\phi$$

Thus,

$$D_\theta = \frac{2\pi U_{max\theta}}{P_\theta} \tag{4.5}$$

$$D_\phi = \frac{2U_{max\phi}}{P_\phi} \tag{4.6}$$

Therefore, the total directivity of the cylindrical antenna for the center frequency is $D_{tot} = D_\phi D_\theta = \frac{4\pi U_{max\theta} U_{max\phi}}{P_\theta P_\phi}$.

4.3.6 Parabolic reflector inside parallel plate

The parabolic reflector that is placed in the waveguide plates is simulated in G2DMULT, and the excitation is along the z-axis, while the design is along xy axes. The simulation in G2DMULT is fast and the results are accurate.

The initial focal point of the parabolic reflector is located in the middle of the waveguide aperture. However, in reality the focal points of the reflector are two and one of them has its coordinates on the edges of the waveguide wall. The y coordinate is equal with the waveguide length and the x coordinate is equal with half of the waveguide width, in both positive and negative direction. Therefore, from a geometrical point of view, the schematic is consisted of two half parabolic reflectors, one in the positive direction and one in the negative direction. The space between them is covered by the waveguide that is inserted.

In order to have high directivity and low sidelobes the focal point of the reflector should be located at the phace center of the feed. After the calculation of the phase center, new changes are made in the design, so that it can coincide with the focus. Firstly, the reflector is shifted again along x-axis, both in the positive and negative dimension a distance that is determined by the x-coordinate of the phase center. Then, depending on whether the phase center is located higher or lower than the focal point, the waveguide should decrease or increase in length respectively, by a factor that equals the difference of the phase center and the focal point.

In that way, by shifting the reflector along the x - axis and by increasing or reducing the waveguide length, the phase center can coincide with the focal point of the reflector. It should be noticed that in reality the phase center is not one single point, but a cluster of different points, but the way of calculating the phase center that was analyzed in chapter 3.3 is a good approximation to locate the phase center in the two dimensional design. The complete reflector design can be seen in figure 4.35.

The radiation pattern of the reflector is also shown in figure 4.36 for the center frequency. The ETSI class 2 and class 3 sidelobe level is also plotted in the same figure. It is noticed that the radiation pattern of this reflector is close to the requirements of the sidelobe levels. Furthermore, the radiation patterns of five difeerent frequencies in the E-band are plotted in figure 4.37. The frequencies that are included are 71, 74.75, 78.5, 82.25 and 86 GHz.

Finally, the radiation patterns of the lowest and the highest frequencies in the E-band are plotted together in 4.38 and its is noticed that the radiation pattern of the reflector is better for higher frequencies and worse for lower frequencies.

The same antenna was designed in HFSS as well and the simulation results are similar with the ones of G2DMULT. The geometry of the antenna designed in HFSS is shown

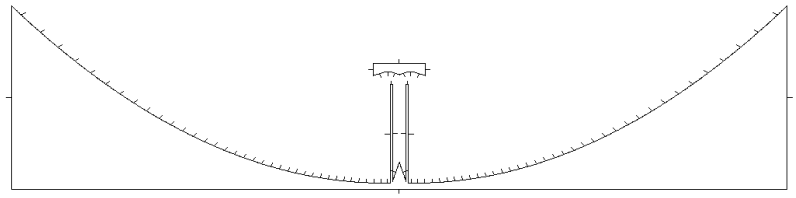

Figure 4.35: One dimensional reflector inside parallel plates

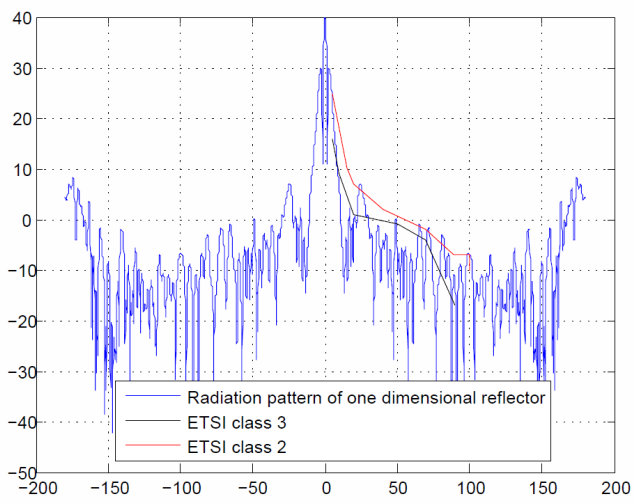

Figure 4.36: Radiation pattern of the one dimensional reflector designed in G2DMULT for f = 78.5GHz

in figure 4.39 and the symmetry of the design has been taken into consideration. The thickness of the antenna is assumed to be very small, around $\lambda/10$ and the antenna is designed among two perfect E planes. The HFSS simulation time is similar to the one of G2DMULT, because of the advantage of the symmetry.

The radiation pattern of the one dimensional reflector antenna that is implemented in HFSS for the center frequency is shown in figure 4.40 and the radiation patterns of the same antenna for the edge frequencies are shown in figure 4.41. Finally, the radiation patterns for 5 different frequencies in the E-band (71, 74.75, 78.5, 82.25 and 86 GHz) are plotted together in figure 4.42.

The similarity in the results of G2DMULT and HFSS is obvious and the conclusion

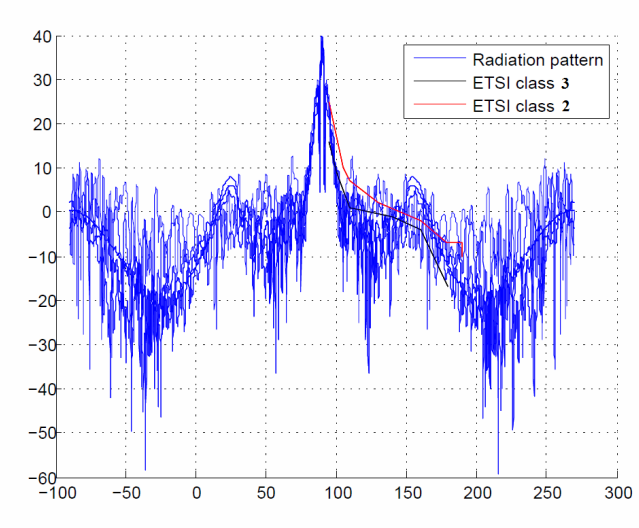

Figure 4.37: Radiation pattern of the one dimensional reflector designed in G2DMULT for f = 71, 74.75, 78.5, 82.25 and 86 GHz

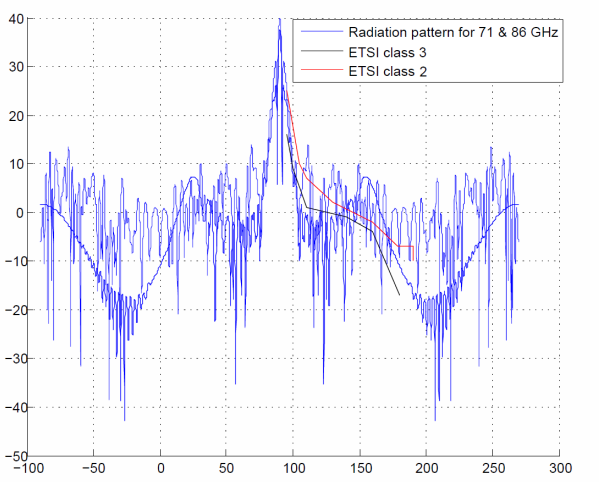

Figure 4.38: Radiation pattern of the one dimensional reflector designed in G2DMULT for f = 71 and 86 GHz

is that the lower frequencies lead to a radiation pattern with higher sidelobes and less directivity and the higher frequencies provide low sidelobes and high directivity.

The directivity of this reflector is calculated by equation 4.6 and the results is D_ϕ = 20.7 dBi for the center frequency of 78.5 GHz.

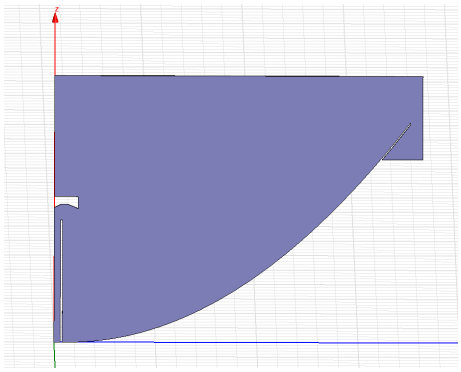

Figure 4.39: Design of the one dimensional reflector in HFSS

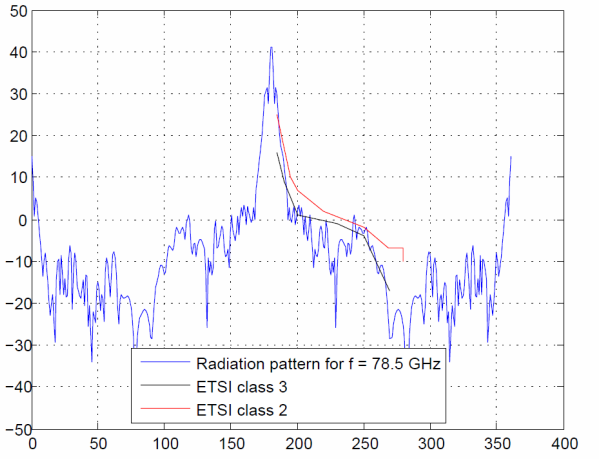

Figure 4.40: Radiation pattern of the one dimensional antenna designed in HFSS for the center frequency

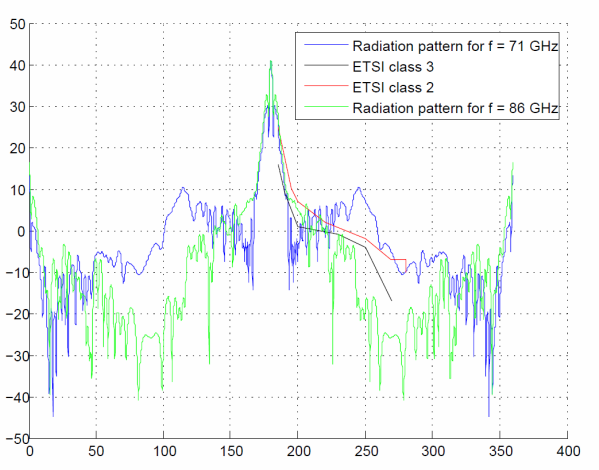

Figure 4.41: Radiation pattern of the one dimensional antenna designed in HFSS for f = 71 GHz and f = 86 GHz

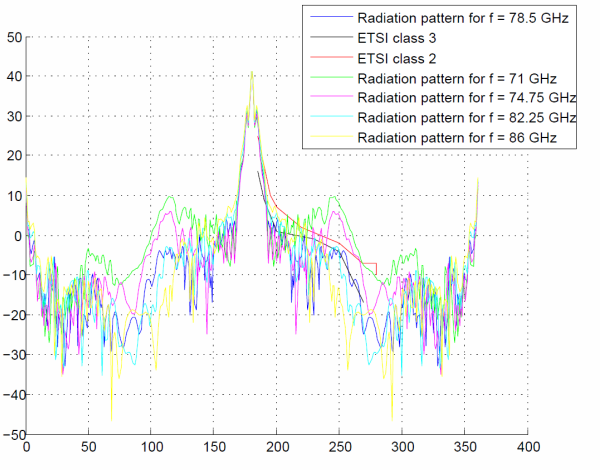

Figure 4.42: Radiation pattern of the one dimensional antenna designed in HFSS for f = 71 - 86 GHz with a step of 3.75 GHz

4.3.7 Cylindrical reflector

Similarly with the one dimensional parabolic reflector that is placed inside the parallel plates, the focal point of the cylindrical reflector should coincide with the phase center. The cross - section of the cylindrical reflector that is designed in G2DMULT is shown in figure 4.43. In that case, the excitation is along the x-axis.

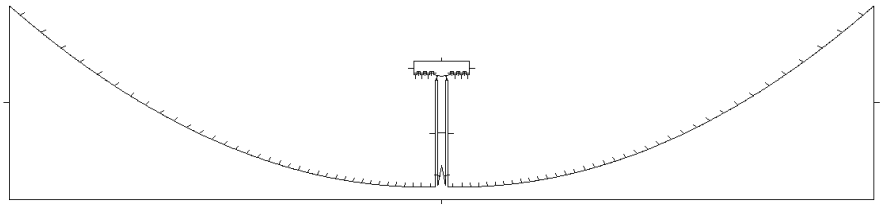

Figure 4.43: Schematic of the cylindrical reflector

The radiation pattern of the complete reflector for the center frequency is plotted in figure 4.44 together with the ETSI class 2 and 3 sidelobe level. It is noticed that the sidelobe level is not satisfied and due to the inaccuracy of G2DMULT for that case, as it was discussed in chapter 4.3.4, the cylindrical reflector is analyzed in HFSS as well.

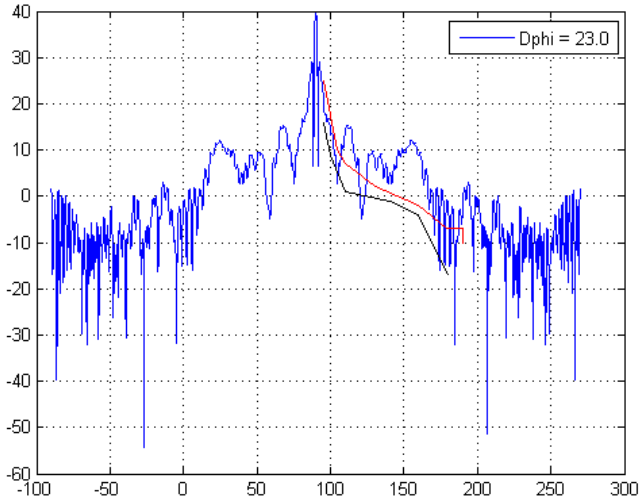

Figure 4.44: Radiation pattern of the cylindrical reflector from G2DMULT at 78.5 GHz

In the same way as the corrugated hat feed, the cylindrical reflector is assumed to be a two dimensional design and it is placed between two perfect magnetic planes. As it was mentioned, in HFSS one can take advantage of the symmetry of the design and this

can reduce the time of the simulations. Radiation boundaries are applied at the rest of the faces and the design is shown in figure 4.45.

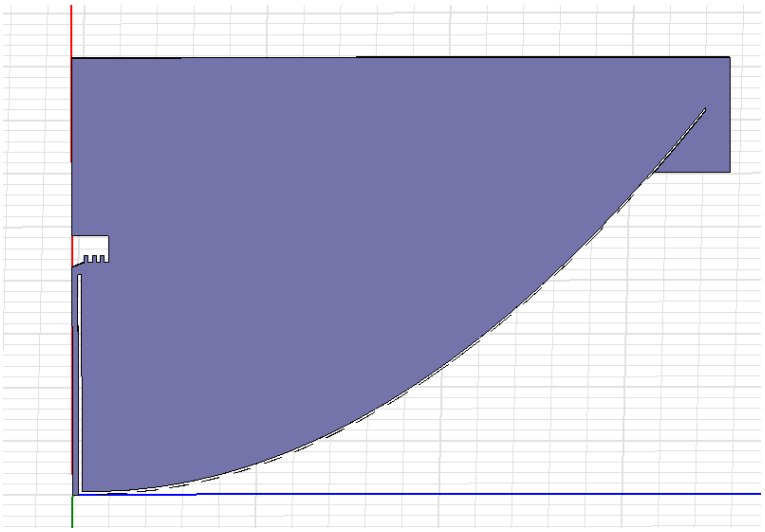

Figure 4.45: Cylindrical reflector designed in HFSS, with an applied symmetry axis

The upper corner of the reflector is designed in such a way, so that the diffraction that might occur on the edge of the reflector could not affect so much the result of the radiation pattern. The radiation pattern of the reflector for the center frequency is plotted in figure 4.46, together with the ETSI class 2 and 3 sidelobe level.

The result of the radiation pattern is different from the one in figure 4.44, but the far - out sidelobes are still high and this can be due to the diffractions from its corners.

Furthermore, the radiation patterns of 5 different frequencies in the E-band, with a step of 3.75 GHz between them are plotted together and the result is presented at figure 4.47.

The directivity of this reflector is calculated by equation 4.5 and it is found to be $D_\theta = 20.7$ dBi for the center frequency of 78.5 GHz. Thus, the total directivity of the cylindrical reflector is calculated in equation 4.7.

$$D_{tot} = D_\phi + D_\theta = 41.4dBi \tag{4.7}$$

The theoretical directivity of the circular reflector is around 43 dBi for the center frequency of 78.5 GHz, as it is shown in figure 3.10. The total aperture efficiency was calculated to be around $0.603 = -2.2dB$ from table 4.5. Therefore, the theoretical directivity minus the aperture efficiency gives the result of the directivity of the cylindrical reflector, that is calculated in equation 4.7.

The material that is used in the simulations of the complete cylindrical reflector in both G2DMULT and HFSS, is perfect electric conductor and no losses are taken into consideration. The fade margin of 2dB between the directivity and the gain requirement of the project is enough to include the losses of a selected conducing material.

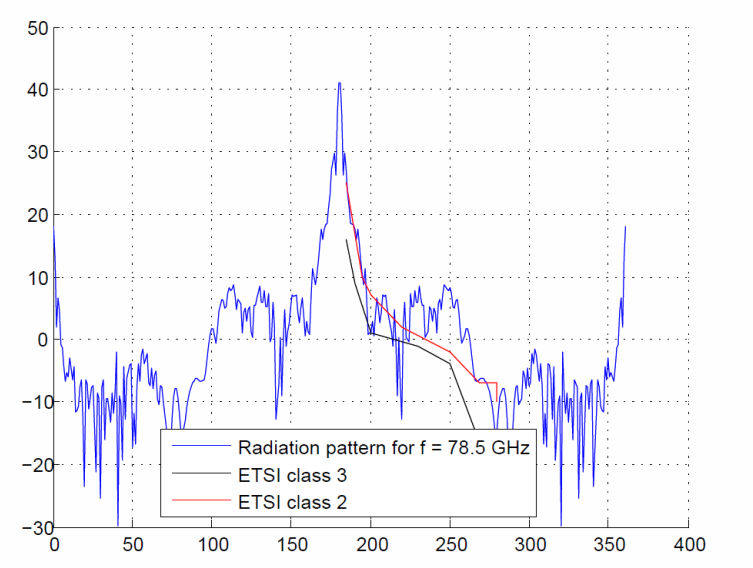

Figure 4.46: Radiation pattern of the cylindrical reflector analyzed in HFSS at 78.5 GHz

Tthe directivity of the cylindrical reflector antenna in the E-band range is shown in figure 4.48. The loss that each subefficiency is causing to the directivity is also shown in the same figure. Similar to the case of the circular reflector, the calculated directivity from the simulations is not exactly the same with the result of the theoretical directivity of a uniform aperture minus the aperture efficiency. This is due to phase errors and high sidelobes that are noticed in the higher frequencies of the E-band.

Finally, a summary of the antenna parameters for both designs is shown in tables 4.6 and 4.7, for the circular and the cylindrical reflector respectively. The dimensions of the antennas and their feeds are shown in detail in the Appendix.

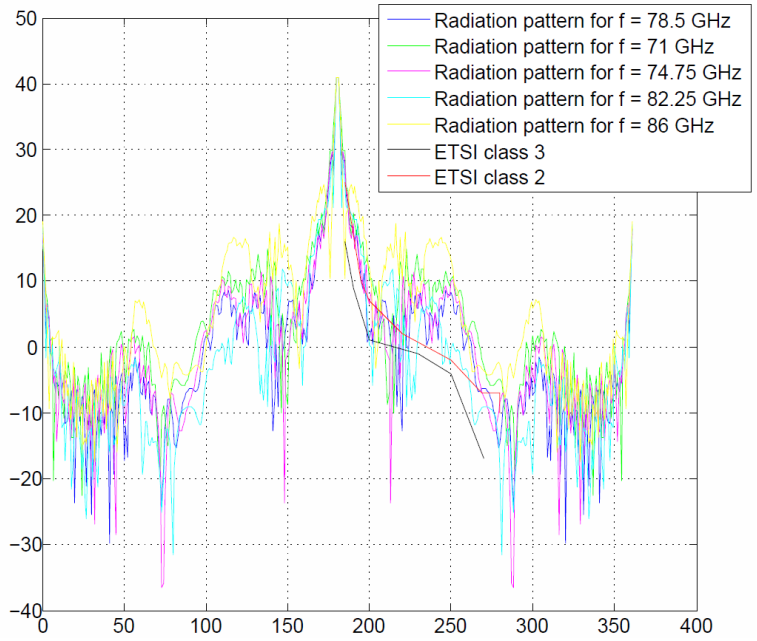

Figure 4.47: Radiation pattern of the cylindrical reflector for f = 71 - 86 GHz with a step of 3.75 GHz

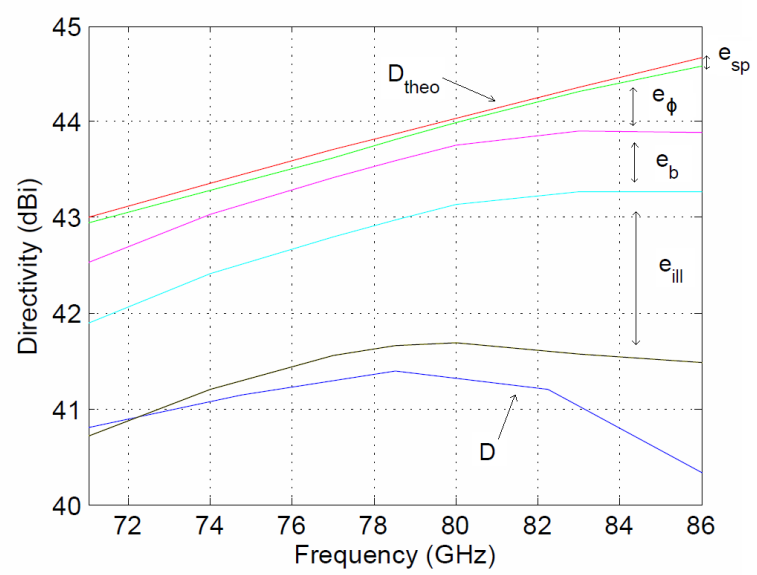

Figure 4.48: Directivity and subefficiencies of the cylindrical reflector for f = 71 - 86 GHz

Parameter	**Value**
Diameter (d)	190 mm
Focus (F)	36.5 mm
Half subtended angle (θ_0)	105°
Depth of focus (Δz)	61.9 mm
Directivity D_0 in the E-band without taper	43 dBi - 44.67 dBi
Aperture efficiency e_{ap}	0.41 - 0.56
Spillover efficiency e_{sp}	0.94 - 0.97
Illumination efficiency e_{ll}	0.65 - 0.67
Polarization sidelobe efficiency e_{pol}	0.69 - 0.93
Phase efficiency e_{ll}	0.99 - 0.93
Blockage efficiency e_b	0.98
Directivity D in the E - band	36.9 dBi - 42 dBi

Table 4.6: Circular parabolic reflector final results

Parameter	**Value**
Length (L)	168.4 mm
Focus (F)	32.3 mm
Half subtended angle (θ_0)	105°
Depth of focus (Δz)	54.85 mm
Directivity D_0 in the E-band without taper	43 dBi - 44.67 dBi
Aperture efficiency e_{ap}	0.59 - 0.48
Spillover efficiency e_{sp}	0.98 - 0.99
Illumination efficiency e_{ll}	0.76 - 0.66
Polarization sidelobe efficiency e_{pol}	1
Phase efficiency e_{ll}	0.85 - 0.95
Blockage efficiency e_b	0.87
Directivity D in the E - band	40.8 dBi - 40.3 dBi

Table 4.7: Cylindrical parabolic reflector final results

5

Tolerance analysis

The position of the hat is very important, in hat feed antennas, because an error in manufacturing might give different directivity results, which are usually worse than the ones that occur from the simulations. A limited tolerance study is done in this section, by shifting the position of the hat for each reflector antenna and notice how this will affect the directivity. The tolerance analysis is done for the center frequency of 78.5 GHz.

5.1 Circular reflector

In the design of the circular reflector the hat is located in a distance of 1.5 mm above the circular waveguide. Therefore, by shifting the hat 0.5 mm along the waveguide direction, both upwards and downwards, in a step of 0.1 mm the radiation pattern of the feed variates, as is is shown in figures 5.1 and 5.2 for the E and H plane.

The variation in the radiation patterns of the circular reflector is shown in figure 5.3. The green curve is the radiation patten for the center frequency when the hat feed is in its initial position and the blue curves show the different shape of the radiation pattern, when the hat of the reflector is shifted up and down.

Moreover, the different losses in directivity are shown in figure 5.4, for different hat positions. The maximum directivity is when the hat feed is not shifted at all, otherwise the directivity loss is 1-1.5dB.

Finally, the return loss changes when the position of the hat changes and the different values of the return loss for the center frequency are shown in figure 5.5, for different hat positions.

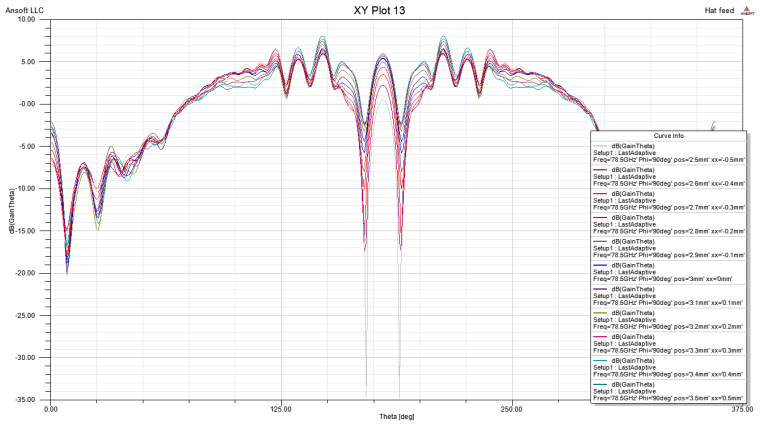

Figure 5.1: Radiation pattern of the E - plane of the circular hat feed, with an applied tolerance in changing the position of the hat 0 - 0.5 mm, upwards and downwards

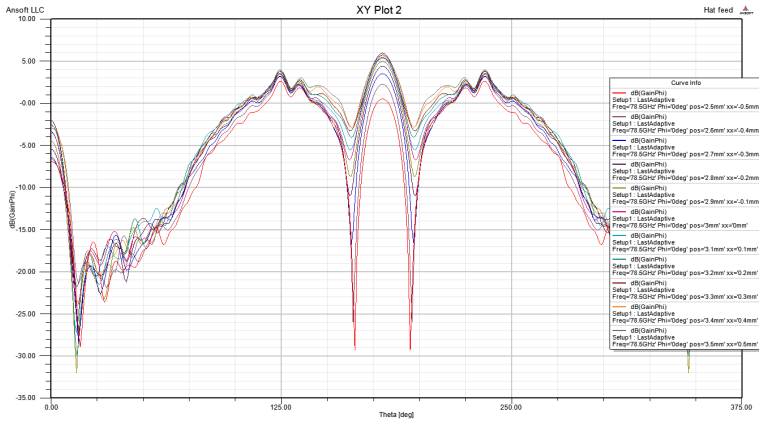

Figure 5.2: Radiation pattern of the H - plane of the circular hat feed, by changing the position of the hat 0 - 0.5 mm, upwards and downwards

5.2 Cylindrical reflector

The same procedure is done for the hat feeds of the cylindrical reflector. Firstly, the hat feed of the one dimensional reflector inside the parallel plate is shifted up and down in the range of -0.5 mm to 0.5 mm with a step of 0.1 mm. The variation at the radiation pattern of the reflector is shown in figure 5.6.

Furthermore, the hat feed of the cylindrical reflector is shifted, as well in the same position range and the radiation pattern variation is shown in figure 5.7. In both case, its is noticed that the more the hat feed is misplaced, the higher the sidelobes appear in the radiation patterns of the reflectors.

Finally, the total directivity of the cylindrical reflector is calculated and its variation

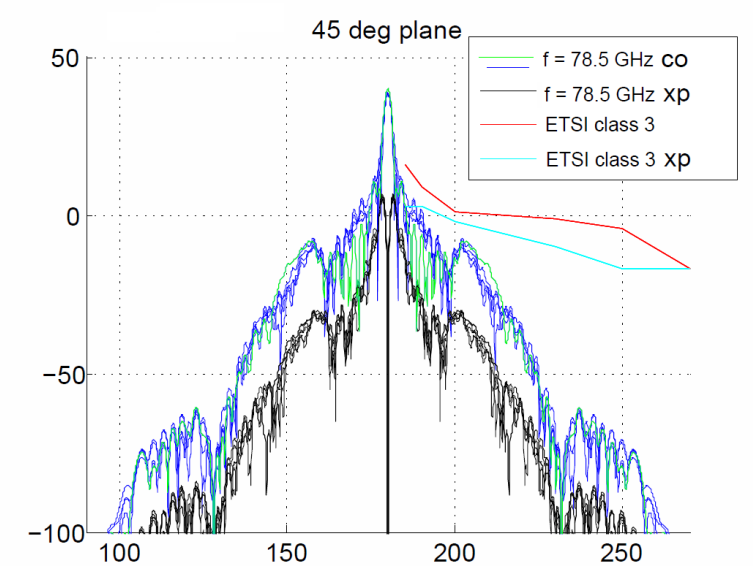

Figure 5.3: Radiation pattern of the 45° - plane of the circular parabolic reflector, by changing the position of the hat 0 - 0.5 mm, upwards and downwards

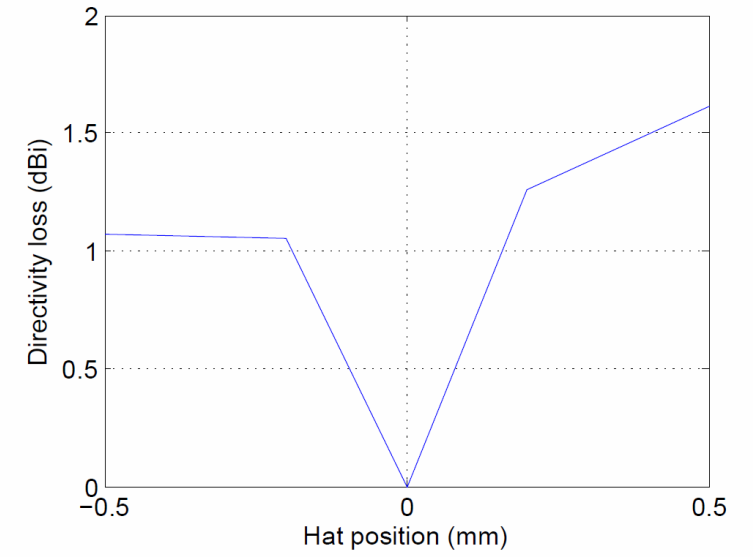

Figure 5.4: Different loss for different hat positions at the center frequency of 78.5 GHz

with the hat position is plotted in figure 5.8. The highest directivity is found to be, when the hat is in its initial position, as it was expected.

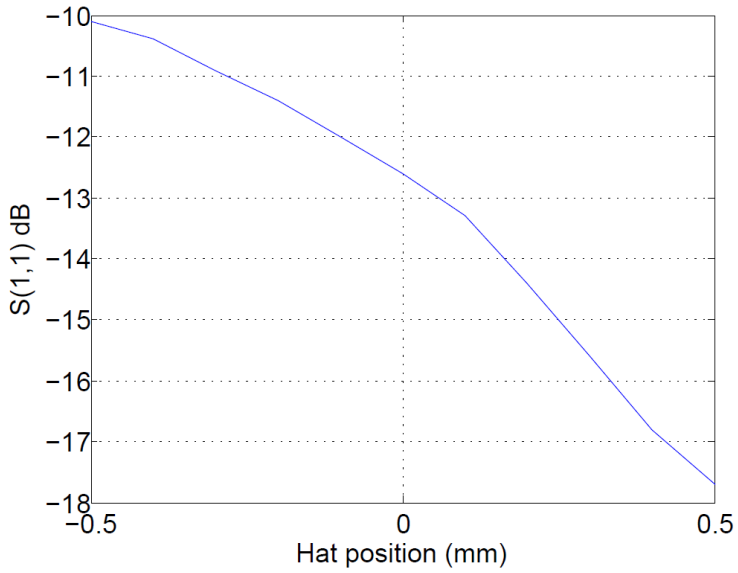

Figure 5.5: Reflection coefficient for different hat positions at 78.5 GHz

Figure 5.6: Radiation pattern of the one dimensional reflector inside the parallel plate, by changing the position of the hat 0 - 0.5 mm, upwards and downwards

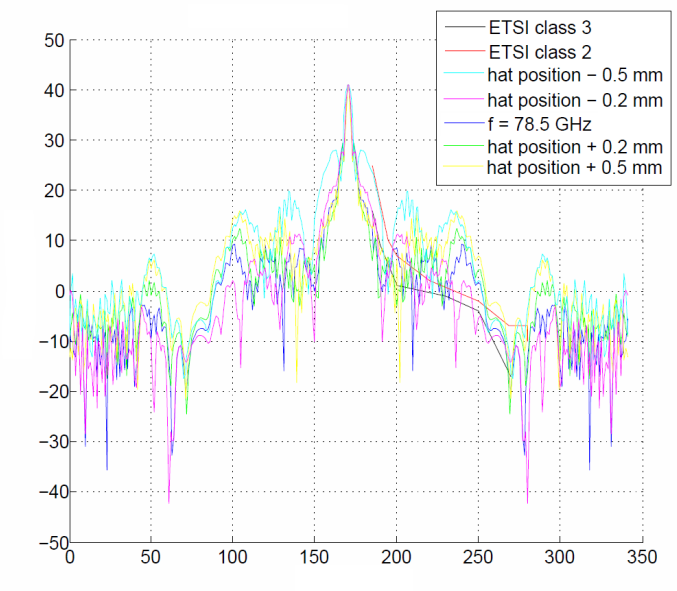

Figure 5.7: Radiation pattern of the cylindrical reflector, by changing the position of the hat 0 - 0.5 mm, upwards and downwards

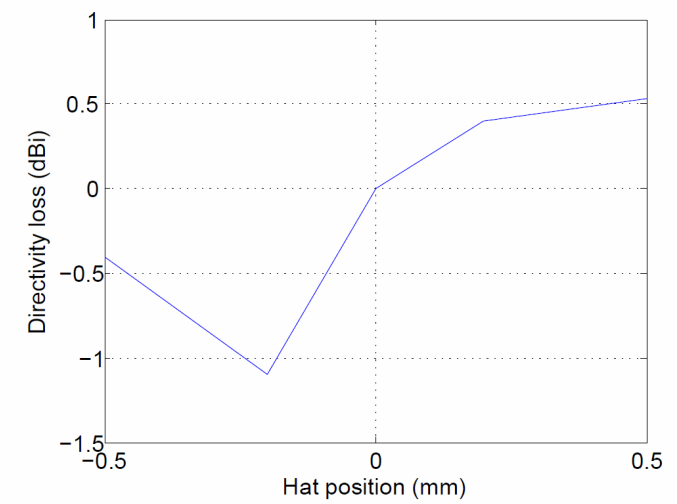

Figure 5.8: Directivity loss for different hat positions at the center frequency of 78.5 GHz

5.3 Surface tolerances

Usually, in reflector antennas the surface does not have the ideal geometrical shape of a perfect paraboloid, but there might be a surface error that is caused by the manufacturing of the antenna. Because of that the phase loss is higher and it can be estimated by equation (5.1) [39].

$$e_{tot} = 1 - (2k\Delta z_{rms})^2 \tag{5.1}$$

where $\Delta z_{rms} = \sqrt{(\boldsymbol{\Delta z})^2 - (\boldsymbol{\Delta z})^2}$ is the weighted root mean - square (RMS) of the surface error around the mean surface error.

The total efficiency and the total loss that the surface tolerance is causing in the reflector antenna depends on the RMS surface error and this relation is shown in figure (5.9). Therefore, for a loss of -0.5 dB, the RMS surface error should be around 0.08 mm.

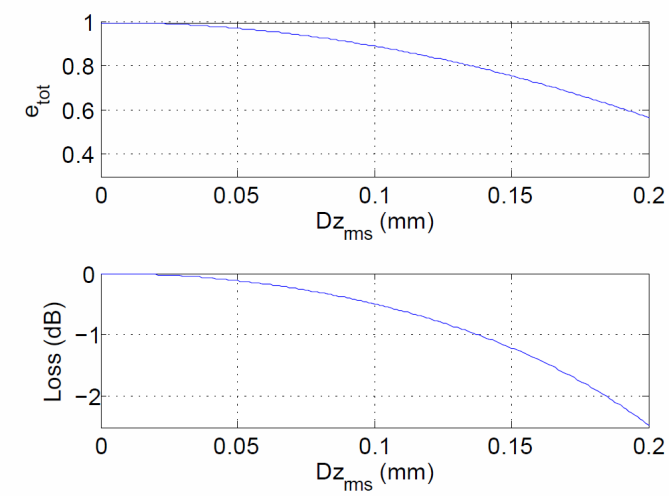

Figure 5.9: Total loss and efficiency of a reflector antenna towards the RMS surface error

6

Conclusion

The need of high data rates and the investigation of wireles solutions as an alternative to fiber optics, led to the design of antennas in very high frequencies. Several antennas that have been already manufactured in the newly allocated E-band (71 - 86 GHz) were presented and two reflector antennas were selected to be designed.

The selected candidates were a parabolic reflector and a cylindrical reflector, whose feed was illuminated by a parallel plate structure that consisted of an one dimensional reflector. The illumination of all reflectors was done with hat feeds, which have many advantages in comparison with other feed structures, because these are self supported and they provide low blockage, low sidelobes and low cross polarization.

Simulations of the antennas were done in HFSS and G2DMULT and the results were found to be adequate to the initial requirements of the project. The circular parabolic reflector has a directivity of 38.4 - 42.1 dBi and the aperture efficiency varies from 0.42 - 0.58 as a function of frequency. The ETSI class 3 sidelobe level is fulfilled in all cases and the return loss is higher or equal to 10 dB for most of the frequencies in the E-band.

The cylindrical reflector gives a directivity of 40.6 dBi for the center frequency and an aperture efficiency of 0.6. The ETSI class 3 sidelobe level is not fulfilled in all cases, but the return loss is close to 10 dB. Some tolerances of the antennas were also studied and future work would include the manufacturing and measurements of both antennas.

7

Future work

The main future work on this project has to do with the manufacturing of the two designed antennas and the measuring of their scattering parameters and radiation patterns. Besides that part some more future work can be done in case the optimum design is desired to be achieved before the manufacturing stage.

The hat feed of the circular reflector antenna can be optimized, so that the E and H planes can become as similar as possible in order to improve the polarization sidelobe efficiency and reduce the phase errors in the radiation patterns of the circular reflector. In that way, the coordinates of the phase center would not only minimize the errors in the 45°-plane, but in the other planes as well.

Furthermore, the ETSI class 3 sidelobe level performance can be improved in the case of the cylindrical reflector, if an optimization procedure is applied not only on the hat feed of the antenna, but on the complete reflector designs as well. However, in reality, some parallel walls are added on the edges of the reflectors in order to reduce the far out sidelobes and improve the radiation pattern.

Finally, in order to fulfill the requirement of the project, which is to have a rectangular waveguide as a connector interface, a transition from circular to rectangular waveguide should be added in the bottom of the feed of the circular reflector when and if it is manufactured.

8

Appendix

In this section the detailed parameters of both antenna designs are shown in mm dimensions, indented to be practical for possible future manufacturing of the antennas.

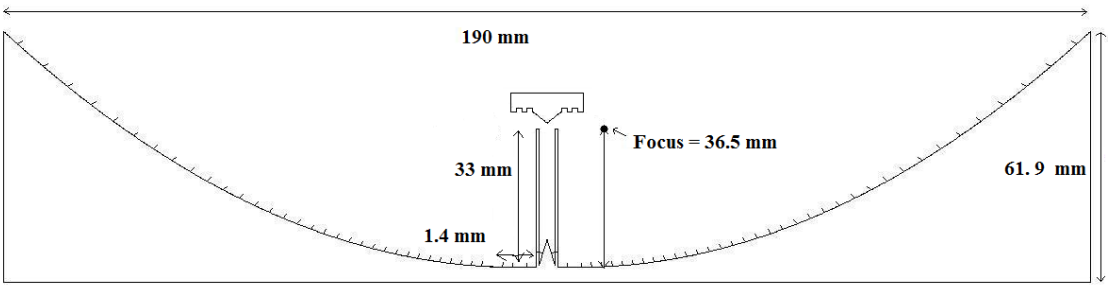

Figure 8.1: Cross section of the circular parabolic reflector

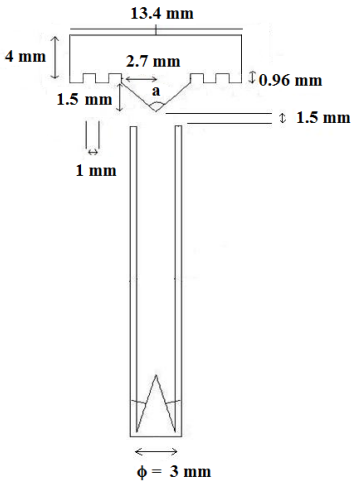

Figure 8.2: Cross section of the circular hat feed of the circular parabolic reflector with a = 84°

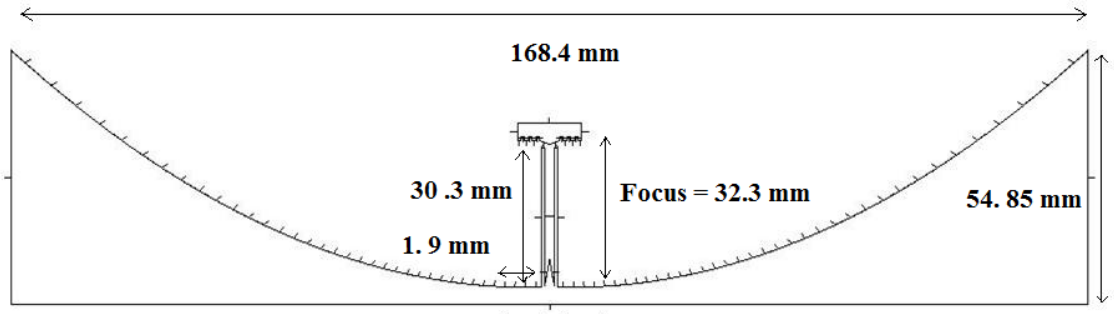

Figure 8.3: Cross section of the cylindrical reflector

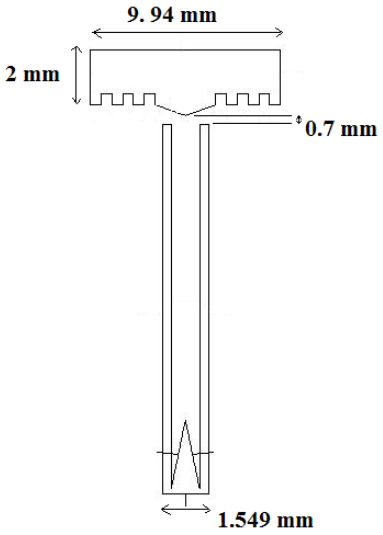

Figure 8.4: Cross section of the linear corrugated feed and the parallel plate of the cylindrical reflector

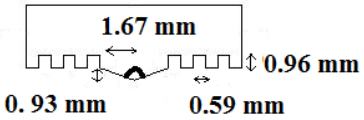

Figure 8.5: Cross section of the linear corrugated feed of the cylindrical reflector, with a cone angle of 122°

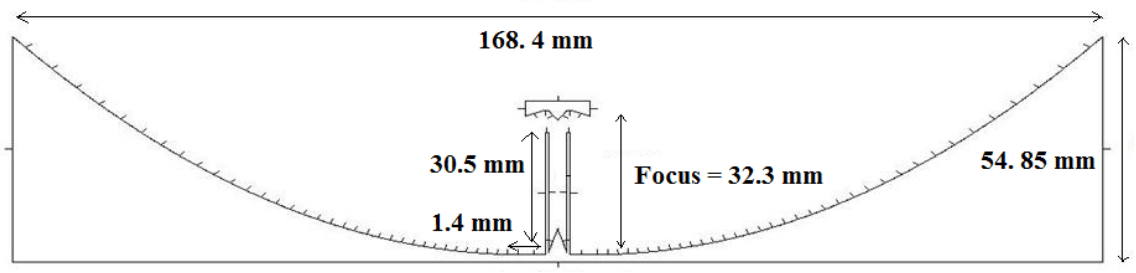

Figure 8.6: Cross section of the one dimensional reflector among the parallel plate

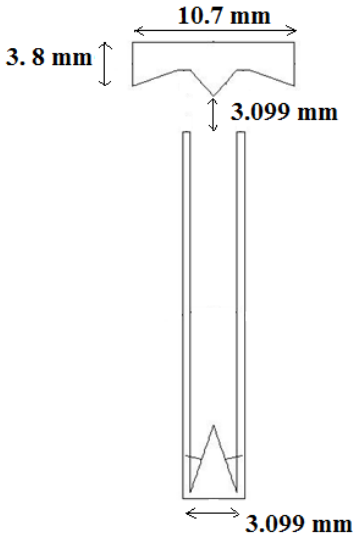

Figure 8.7: Cross section of the hat feed and the waveguide of the one dimensional reflector among the parallel plate

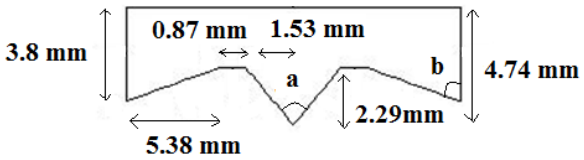

Figure 8.8: Cross section of the hat feed of the one dimensional reflector among the parallel plate, where a = 67.5° and b = 65.5°

Bibliography

[1] V. Dyadyuk, J. D. Bunton, Y. J. Guo, Study on high rate long range wireless communications in the 71 – 76 and 81 – 86 GHz, 2009 EuMA (2009) 1315 – 1318.

[2] V. Dyadyuk, Y. J. Guo, J. D. Bunton, Multi - gigabit wireless communication technology in the E - band, IEEE (2009) 137 – 141.

[3] E. E. . 217-4-2, Fixed radio systems; Characteristics and requirements for point - to - point equipment and antennas; Part 4-2: Antennas; Harmonized EN covering the essential requirements of arcticle 3.2 of R&TTE directive, ETSI v.1.5.1 (2010 - 01) 2 – 35.

[4] M. Floreani, G. Aulisio, M. Frecassetti, Design and experimental validations of a 70 GHz cassegrain antenna with a shaped subreflector geometry, 2002 IEEE (2002) 584 – 587.

[5] G. Aulisio, H. Palacios, J. Vassallo, A 70 GHz Cassegrain antenna using a fresnel reflector.

[6] F. Schafer, F. Gallee, G. Landrac, M. Ney, Optimum reflector shapes for anticollision radar at 76 GHz, Microwave and Optical technology letters Vol. 24, No. 6 (March 20 2000) 400 – 404.

[7] M. Enlund, M. Sadrai, A. Derneryd, U. Engstrom, M. Johansson, B. Svensson, Parallel plate waveguide antenna for point - to - multipoint communication at millimeter-wave frequencies, Electronics letters Vol. 41.

[8] A. Nesic, I. Radnovic, 60 ghz range high gain printed antenna array with a cylindrical-parabolic reflector Volume 64 (March 2011) 48 – 51.

[9] D. Neculoiu, S. I. Ene, A. A. Muller, C. Buiculescu, Electromagnetic modeling and design of 77 GHz antennas in LTCC technology, 2009 IEEE (2009) 341 – 344.

[10] M. El-Nawawy, D. Korzec, W. Mahler, The design of 80 GHz antenna array on LTCC substrate, 2011 IEEE GCC Conference and Exhibition (GCC) (February 19-22, 2011, Dubai, United Arab Emirates) 217 – 220.

[11] A. Rida, M. Tentzeris, S. S. Nikolaou, Design of low cost microstrip antenna arrays for mm-wave applications, IEEE (2011) 2071 – 2073.

[12] M. Stotz, G. Gottwald, H. Haspeklo, J. Wenger, Planar millimeter - wave antennas using SiNx - Membranes on GaAs, IEEE (1996) 1593 – 1595.

[13] M. Stotz, G. Gottwald, H. Haspeklo, J. Wenger, Planar single- and dual - polarized aperture coupled E-band antennas on GaAs using SiNx - Membranes, IEEE (1996) 1540 – 1543.

[14] V. Volkov, M. Parnes, V. Korolkov, A low cost pencil - beam microstrip antenna at 76.5 GHz, Technical Feature.

[15] N. Nikolic, A. Weily, Compact E - band planar quasi - Yagi antenna with folded dipole driver, IET Microwaves, Antennas & Propagation Vol. 4 (2010) 1728 – 1734.

[16] F. Kolak, C. Eswarappa, A low profile 77 GHz three beam antenna for automotive radar, IEEE (2001) 1107 – 1110.

[17] H. S. Lee, J. G. Kim, S. Hong, J. B. Yoon, Micromachined CPW-fed suspended patch antenna for 77 GHz automotive radar applications.

[18] T. Komljenovic, Lens antennas - Analysis and synthesis at mm-waves.

[19] E. B. Lima, J. R. Costa, C. A. Fernandes, Broadband reflector fed by integrated lens antenna with frequency constant directivity, IEEE.

[20] A. Neto, I. E. Lager, Non. dispersive, UWB leaky lens antenna for millimeter and sub-millimeter wave frequencies.

[21] H. Kobayashi, Y. Yoshizumi, Receiving properties of extended hemispherical lens coupled slot antennas for 94 - GHz millimeter wave radiation, Electronics and communications in Japan, Part 1 Vol. 84 (2001) 1211 – 1219.

[22] B. Fuchs, O. Lafond, S. Rondineau, M. Himdi, L. Le Coq, Design and characterisation of half - Maxwell fish - eye lens antenna in 76 - 81 GHz band, Electronics letters Vol.42.

[23] M. Gueye, H. Ouslimani, S. Burokur, A. Priou, Y. Letestu, A. Bayon, Antenna array for point - to - point communications in E - band frequency range, IEEE (2009) 2077 –2079.

[24] R. Shireen, T. Hwang, S. Shi, D. W. Prather, Stacked patch excited horn antenna at 94GHz, Microwave and Optical technology letters Vol.50 (2008) 2071 – 2073.

[25] A. I. Zaghloul, T. K. Anthony, A 76 - GHz antenna with highly - tapered aperture for collision avoidance systems 510 – 514.

[26] T. M. Grzegorczyk, A. A. Melcon, J. F. Zurcher, A. K. Skrivervik, P. Renaud, J. R. Mosig, Integrated SSFIP - horn antenna 75 GHz, Microwave and Optical technology letters Vol. 26 (2000) 298 – 302.

[27] T. M. Grzegorczyk, J. F. Zurcher, P. Renaud, J. R. Mosig, Micromachined horn antenna operating at 75 GHz.

[28] M. M. Kangas, M. Ansmann, K. Copsey, B. Horgan, R. Leonardi, P. Lubin, T. Villela, A 100 - GHz high - gain tilted corrugated nonbonded platelet antenna, IEEE Vol.4 (2005) 304 – 307.

[29] J. Hirokawa, M. Ando, 76 GHz post-wall waveguide fed parallel plate slot arrays for car - radar applications, IEEE (2000) 98 – 101.

[30] J. Hirokawa, M. Ando, Sidelobe suppression in 76 GHz post-wall waveguide-fed parallel-plate slot arrays, IEEE Vol.48 (2000) 1727 – 1732.

[31] J. Hirokawa, M. Ando, Model antenna of 76 GHz post - wall waveguide fed parallel plate slot arrays, IEEE (1999) 146 – 149.

[32] Y. Kimura, J. Hirokawa, M. Ando, Low sidelobe single-layer slotted waveguide arrays at 76 GHz band, IEEE (2000) 86 – 89.

[33] T. Shijo, S. Obayashi, T. Morooka, Design and development of 77 - GHz pair - slot array antenna with single-mode post-wall waveguide for automotive radar, IEEE (2011) 476 – 479.

[34] M. Zhang, J. Hirokawa, M. Ando, An E-band partially corporate feed uniform slot array with laminated quasi double-layer waveguide and virtual PMC terminations, IEEE Vol.59 (2011) 1521 – 1527.

[35] M. Ettorre, R. Sauleau, L. Le Coq, F. Bodereau, Single-folded leaky-wave antennas for automotive radars at 77 GHz, IEEE Vol.9 (2010) 859 – 862.

[36] S. Cheng, H. Yousef, H. Kratz, 79 GHz slot antennas based on substrate integrated waveguides (siw) in a flexible printed circuit board, IEEE Vol.57 (2009) 64 – 71.

[37] H. Uchimura, T. Takenoshita, A ceramic planar 77 GHz antenna array, IEEE (1999) 453 – 456.

[38] Y. Kimura, J. Hirokawa, M. Ando, M. Haneishi, Alternating-phase fed single-layer slotted waveguide arrays with wide chokes at 76 GHz band, IEEE (2002) 228 –231.

[39] P. S. Kildal, Foundations of Antennas - A unified approach for line - of - sight and multipath, Chalmers, 2009.

[40] P. S. Kildal, Aperture efficiency and line feed phase center of parabolic cylindrical reflector antenna, IEEE Vol. AP-32 (June 1984) 553 – 561.

[41] J. Yang, P. S. Kildal, Calculation of ring-shaped phase centers of feeds for ring-focus paraboloids, IE Vol.48 (April 2000) 524 – 528.

[42] J. Yang, P. S. Kildal, Calculation of phase centers of feeds for reflectors when the phase variations are large, 1998 IEEE AP-S International Symposium.

[43] http://www.ansys.com/products/simulation+technology/electromagnetics/high-performance+electronic+design/ansys+hfss.

[44] J. Yang, U. Caldberg, P. S. Kildal, M. Ng, A fast mode analysis for waveguides of arbitrary cross section with multiple regions by using a spectrum of two-dimensional solutions and asymptotic waveform evaluation, IEEE Trans. on MTT vol. 52, no. 6 (June, 2004) 590 – 600.

[45] J. Yang, P. S. Kildal, A fast calculation of impedances of dipoles near cylindrical structure by applying asymptotic waveform evaluation in a spectrum of 2d solutions, Microwave Opt. Tech. Lett. vol. 43, no. 4 (Nov. 2004) 314–317.

[46] J. Yang, P. S. Kildal, On the odd-even property of functions for boundary currents over kz in a spectrum of two-dimensional solutions, IEEE Antennas Wireless Propagat. Lett. vol. 4 (Aug. 2005) 281–284.

[47] J. Yang, P. S. Kildal, A fast algorithm for calculating the radiation pattern in the longitudinal plane of antennas with cylindrical structure by applying asymptotic waveform evaluation in a spectrum of two-dimensional solutions, IEEE Trans. on Antennas Propagat. vol. 52, no. 7 (July, 2004) 1700 – 1706.

[48] J. Yang, P. S. Kildal, Scattering by screw heads in reflecting surfaces and their effect on the sidelobes of reflector antennas, Microwave Opt. Tech. Lett. vol. 38, no.3 (5 August 2003) 213 – 217.

[49] J. Yang, J. Carlsson, P. S. Kildal, C. Carlsson, Calculation of self impedance and radiation efficiency of a dipole near a lossy cylinder with arbitrary cross section by using the moment method and a spectrum of two-dimensional solutions, Microwave Opt. Tech. Lett. vol. 32, no. 2 (20 Jan. 2002) 108 – 112.

[50] J. Yang, P. S. Kildal, Presentation of the spectral electric and magnetic field integral equations used in g2dmult for analyzing cylindrical structures of multi-material regions, Microwave Opt. Tech. Lett. vol. 34, no. 2 (20 July 2002) 88 – 93.

[51] J. Yang, P. S. Kildal, An efficient computation of impedances of dipoles over cylindrical structure by using a spectrum of 2d solutions with asymptotic waveform evaluation, In Proc. 2004 IEEE AP-S International Symposium, Monterey, California.

[52] J. Yang, P. S. Kildal, Fast calculation of radiation patterns of antennas with cylindrical structure by applying asymptotic waveform evaluation in a spectrum of two-dimensional solutions, In Proc. 2003 IEEE AP-S International Symposium (Columbus, Ohio, June 22-27, 2003) 823 – 826.

[53] U. Caldberg, J. Yang, P. S. Kildal, Moment method solutions of cylindrical waveguides by searching in a spectrum of two-dimensional solutions, In Proc. 2003 IEEE AP-S International Symposium (Columbus, Ohio, June 22-27, 2003) 657 – 660.

[54] P. S. Kildal, T. Jensen, Efficient small reflector with hat feed, ELAB-RUNIT, Norwegian Institute of Technology 154 – 157.

[55] G. E. Geterud, J. Yang, T. Ostling, P. Bergmark, Design and optimization of a compact wideband hat-fed reflector antenna for satellite communications, IEEE Transactions on Antennas and Propagation Vol.60 (2012) 1–8.

[56] W. Wei, J. Yang, T. Ostling, T. Schafer, A new hat feed for reflector antennas realized without dielectrics for reducing manufacturing cost and improving reflection coefficienc, IET Microwaves, Antennas & Propagation Vol. 5, no. 7 (July, 2011) 837–843.

[57] J. Yang, W. Wei, T. Ostling, T. Schafer, A new metal-rod-supported hat antenna for potentially combining with the eleven antenna as a dual-band feed for reflectors, 5th Eur. Conference on Antennas Propagation (EuCAP2011).

[58] J. Yang, P. S. Kildal, Fdtd design of a chinese hat feed for shallow mm-wave reflector antennas, 1998 IEEE AP-S International Symposium.

[59] J. Yang, P. S. Kildal, Gaussian vertex plate improves reflection coefficient and far-out sidelobes in prime-focus reflector antennas, Microwave Opt. Tech. Lett. vol. 21, no. 2 (20 April 1999) 125 – 129.

[60] Circular waveguide sizes, http://www.millitech.com/pdfs/circwave.pdf.

[61] R. E.Collin, Foundations for Microwave Engineering, John Wiley & Sons, 2001.

[62] P. S. Kildal, The hat - feed: A dual - mode rear - radiating waveguide antenna having low cross polarization, IEEE Vol. 35 (1987) 1010 – 1016.

[63] E. Geterud, J. Yang, T. Ostling, Radome design for hat-fed reflector antenna, 6th Eur. Conf. on Antennas Propagat. (EuCAP2012).

[64] E. Geterud, J. Yang, T. Ostling, Wide band hat-fed reflector antenna for satellite communications, In 5th Eur. Conf. on Antennas Propagat. (EuCAP2011).

[65] P. S. Kildal, J. Yang, Fdtd optimizations of the bandwidth of the hat feed for mm-wave reflector antennas, IEEE AP-S International Symposium,Montreal.

[66] Rectangular waveguide sizes, http://www.microwavers.org/waveguide.htm.

[67] http://www.mathworks.com/matlabcentral/fileexchange/24838.